ANALYSIS OF PERIODICALLY-FORCED HOMOGENEOUS TURBULENCE IN THE RAPID DISTORTION LIMIT

A Thesis

by

JOSHUA R. O'NEIL

Submitted to the Office of Graduate Studies of
Texas A&M University
in partial fulfillment of the requirements for the degree of

MASTER OF SCIENCE

December 2004

Major Subject: Aerospace Engineering

ANALYSIS OF PERIODICALLY-FORCED HOMOGENEOUS TURBULENCE IN THE RAPID DISTORTION LIMIT

A Thesis

by

JOSHUA R. O'NEIL

Submitted to Texas A&M University
in partial fulfillment of the requirements
for the degree of

MASTER OF SCIENCE

Approved as to style and content by:

Sharath S Girimaji (Chair of Committee)	Othon K. Rediniotis (Member)
Prabir Daripa (Member)	Walter E. Haisler (Head of Department)

December 2004

Major Subject: Aerospace Engineering

ABSTRACT

Analysis of Periodically-Forced Homogeneous Turbulence in
the Rapid Distortion Limit. (December 2004)
Joshua R. O'Neil, B.A., University of St. Thomas;
B.S., Texas A&M University
Chair of Advisory Committee: Sharath S. Girimaji

Rapid Distortion Theory is used to perform calculations of unsteadily-forced initially isotropic turbulence so that the physics of such flows can be better understood. The results of these calculations show that there are three distinct regimes of physical behavior for the kind of turbulence that we are considering: (1) turbulence that is forced at a relatively low frequency in which the kinetic energy settles down to a constant value at later times, (2) turbulence that is forced at a slightly higher frequency in which the kinetic energy value oscillates for a time, but then increases dramatically, and (3) turbulence that is forced at a relatively high frequency in which the kinetic energy evolution exhibits a periodic behavior. To better understand the role of the rapid pressure-strain correlation, these results are also compared to Inertial Model results for the same set of forcing frequencies. The results of this comparison show that the rapid pressure plays a key role in determining the stability characteristics of unsteadily-forced turbulence. The evolution equation for kinetic energy is then used to propose a model that describes the behavior approximately in terms of a time lag between applied mean strain and the Reynolds stress. This model suggests that the different responses under the different frequencies of forcing correspond to different stress-strain time lags. Overall, then the results indicate that rapid pressure serves to create a time lag between applied stress and strain, and it is the extent of this time

lag that causes turbulence to respond differently under various frequencies of forcing.

To my mother, Lucy O'Neil Hoffart, and in memory of my father, Robert O'Neil

ACKNOWLEDGMENTS

I would like to acknowledge and thank everyone who has helped and supported in various ways in completing this journey. I am indebted first and foremost to my advisor and committee chair, Dr. Sharath S. Girimaji. His early direction during my undergraduate years, and his ongoing teaching, supervision, and direction have made this thesis possible.

My thanks are due to Dr. Eunhwan Jeong for helping me establish my direction through his previous work in this field and his helpful explanations. Similarly, I would like to thank Dr. Svetlana Poroseva for her advice and insight in the early stages of my study. Also, I would like to thank the members of my committee, Dr. Othon Rediniotis and Dr. Prabir Daripa.

I would also like to acknowledge the help and support of my friends and colleagues. I am indebted to Aditya Murthy for his constant help, explanations, insight and friendship over the years. In addition, I would like to thank Steven Chambers for his advice and friendship. Thanks are due to Theresa Spaeth for being there and helping me in all the small ways. Finally I would like to thank Julie Evans for her understanding and support through the whole process.

Finally I would like to thank Ms. Karen Knabe for her assistance in so many areas over the years.

TABLE OF CONTENTS

Page

LIST OF FIGURES

FIGURE Page

CHAPTER I

INTRODUCTION

A. Overview

Control of turbulent flows is a major area of research in the field of fluid dynamics. Turbulent flow control has important utility in both internal and external flows, including drag reduction and mixing enhancement for combustion, among others. Although flow control strategies depend largely on the physical geometry and flow conditions of each particular case, there are fundamental universal features that are common to most flow control problems. To improve flow control strategies, it is necessary to study these universal features.

One particular feature of turbulence that is relevant to flow control is the response of turbulence to external forcing. The present study specifically considers the response of initially isotropic turbulence when subjected to unsteady or periodic forcing. This type of physical situation is commonly found in flow control problems that use synthetic jet actuation to modify the boundary layer in a flow so that separation can be modified. In the problem of periodically-forced turbulence, an initially isotropic turbulent velocity field is subjected to a time-varying mean velocity gradient, and the resulting turbulence is examined. This thesis focuses specifically on determining the impact of unsteady shearing on a turbulent velocity field over a range of different forcing frequencies.

Of particular interest in devising a turbulence control strategy is the response of a turbulent flowfield to unsteady external forcing, the timescale of which is smaller than the characteristic timescale of turbulence. Such forcing can modify the turbulence

---

The journal model is the *Journal of Fluid Mechanics*.

cascade process leading to a desired behavior. The turbulence processes that play a key role in determining the dynamics when subject to such rapidly varying forcing are production and rapid pressure-strain correlation. Therefore in the present study we restrict our attention to the rapid distortion limit of turbulence. In this limit, the governing equations are linear and the resulting analysis is called Rapid Distortion Theory (RDT). In RDT, the turbulent velocity field behaves in an elastic manner rather than a viscous manner, that is, the stresses in a fluid element depend on the total strain, and not on the current strain rate. In addition, due to the linearity of the governing equations, they can be solved much more easily than full nonlinear turbulence treatments. Because of this property of RDT, the problem considered here can be studied in a much more computationally affordable manner.

B. Background and Objectives

This study uses RDT equations to investigate the physical phenomenon of periodically-forced turbulence. RDT has been much used in the past as an effective tool for analyzing turbulence, especially with respect to modeling of the rapid pressure-strain correlation. The most significant RDT analysis of initially isotropic turbulence (Crow, 1968) led to the following rapid pressure-strain correlation model in the RD limit:

$$\Phi_{ij}^{(r)} = -\frac{3}{5}(P_{ij} - \frac{2}{3}P\delta_{ij}) \tag{1.1}$$

This relation was derived assuming initially isotropic turbulence and has been used in subsequent work to help model the rapid pressure-strain correlation term. The most important RDT studies for initially anisotropic turbulence are found in Sreenivasan and Narasimha (1978), Maxey (1982), Hunt and Carruthers (1990), and Girimaji, Jeong, and Poroseva (2003). These studies look at turbulence evolution under vari-

ous different types of rapid deformation and initial anisotropy. Maxey is chiefly concerned with studying the role of the rapid pressure-strain correlation term in the RD limit. He further compares the performance of RDT in the homogeneous shear case to a turbulence model proposed by Launder, Reece, and Rodi (1973). The work of Hunt and Carruthers studies the role of initial and boundary conditions on turbulence evolution. This work indicates that the evolution of initially anisotropic turbulence depends heavily on the level of the initial anisotropy. Girimaji, Jeong, and Poroseva (2003) investigated the evolution of turbulence in the rapid distortion limit for several different initially anisotropic cases. The behavior of the rapid pressure-strain correlation was studied for a variety of different types of strain-dominated deformation. The results of this study indicated that the evolution of turbulence in the rapid distortion limit is dependent not only on the type and level of initial anisotropy, but also on the imposed mean flow deformation. The work also proposed new guidelines for modeling the rapid pressure-strain correlation term based on these findings.

All of the previous work outlined above addresses steady, homogeneous deformation of turbulence in the rapid distortion limit. The present study takes the next step by examining the response of turbulence when subjected to a periodically-varying shear deformation. This study is motivated by two main factors. First, the physical phenomenon of unsteadily-forced turbulence is a situation that is not well understood at present, even in the rapid distortion limit. Developing an understanding of this turbulent regime can conceivably lead to significant practical application in the area of turbulent flow control. Second, as a linear theory, RDT specifically has been shown to be a useful tool and thus it serves as a practical starting point from which to gain a general understanding and description of a particular type of turbulent flow, in this case, unsteadily forced turbulence. Once the RDT physics of this problem are understood, future work can use this understanding as a starting point to focus on

the non-linear physics and geometric flow aspects the problem.

CHAPTER II

RAPID DISTORTION THEORY

A. RDT Background and Derivation of Equations

In Rapid Distortion Theory, the governing equation for the evolution of the fluctuating velocity is derived from the Navier-Stokes equation, which is given by

$$\frac{DU}{Dt} = -\frac{1}{\rho}\nabla p + \nu\nabla^2 U. \tag{2.1}$$

If we decompose the turbulent velocity field into mean and fluctuating parts, the so-called Reynolds decomposition, this gives

$$U(x,t) = \langle U(x,t)\rangle + u(x,t). \tag{2.2}$$

Substituting this decomposition into the Navier-Stokes equation and taking the mean gives the the mean momentum, or the Reynolds-averaged Navier-Stokes (RANS) equations (Pope, 2000). This is the mean velocity evolution equation, and is given by

$$\frac{\overline{D}\langle U_j\rangle}{\overline{D}t} = \nu\nabla^2\langle U_j\rangle - \frac{\partial\langle u_i u_j\rangle}{\partial x_i} - \frac{1}{\rho}\frac{\partial\langle p\rangle}{\partial x_j}. \tag{2.3}$$

In the above equation, $\frac{\overline{D}}{\overline{D}t}$ is the mean substantial derivative defined by

$$\frac{\overline{D}}{\overline{D}t} \equiv \frac{\partial}{\partial t} + \langle U\rangle\cdot\nabla \tag{2.4}$$

Finally, the evolution equation for the fluctuating velocity is found by subtracting the RANS equations (Eq. (2.3)) from the Navier-Stokes equation (Eq. (2.1)), and the result is given by

$$\frac{\overline{D}u_j}{\overline{D}t} = -u_i\frac{\partial\langle U_j\rangle}{\partial x_i} - u_i\frac{\partial u_j}{\partial x_i} + \nu\nabla^2 u_j - \frac{\partial p'}{\partial x_j}. \tag{2.5}$$

In this equation, p' is the fluctuating pressure which is governed by

$$\nabla^2 p' = -2\rho \frac{\partial \langle U_i \rangle}{\partial x_j} \frac{\partial \langle U_j \rangle}{\partial x_i} - \frac{\partial u_i}{\partial x_j} \frac{\partial u_j}{\partial x_i}. \tag{2.6}$$

The pressure is decomposed into two parts: $p' = p^{(r)} + p^{(s)}$, where $p^{(r)}$ is the *rapid pressure*, and $p^{(s)}$ is the *slow pressure*. If we substitute the Reynolds decomposition (Eq. 2.2) into equation (2.6), the equation for the fluctuating pressure can be written as

$$\frac{1}{\rho}\nabla^2 p' = \frac{1}{\rho}\nabla^2 (p^{(r)} + p^{(s)}) = -2\frac{\partial \langle U_i \rangle}{\partial x_j} \frac{\partial u_j}{\partial x_i} - \frac{\partial^2 u_i u_j}{\partial x_i \partial x_j}. \tag{2.7}$$

From this the individual equations for slow and rapid pressure are identified:

$$\frac{1}{\rho}\nabla^2 p^{(r)} = -2\frac{\partial \langle U_i \rangle}{\partial x_j} \frac{\partial u_j}{\partial x_i} \tag{2.8}$$

$$\frac{1}{\rho}\nabla^2 p^{(s)} = -\frac{\partial^2 u_i u_j}{\partial x_i \partial x_j}. \tag{2.9}$$

Note that equations (2.5) and (2.7) are both nonlinear in the fluctuating velocity. For both of these equations, the first term on the right hand side is linear in the fluctuating velocity while the second term is nonlinear.

The relationship between the linear and nonlinear terms can be quantified by a timescale ratio, $\frac{Sk}{\epsilon}$. The term S in this ratio can be viewed as the frequency of the mean flow. It represents the timescale that characterizes the the mean flow as a production mechanism that forces turbulence, and it is is defined by

$$S \equiv \left(2\overline{S}_{ij}\overline{S}_{ij}\right)^{\frac{1}{2}} \tag{2.10}$$

where S_{ij} is the mean rate-of-strain tensor, given by:

$$\overline{S}_{ij} \equiv \frac{1}{2}\left(\frac{\partial \langle U_i \rangle}{\partial x_j} + \frac{\partial \langle U_j \rangle}{\partial x_j}\right). \tag{2.11}$$

The term ϵ/k can be viewed as the characteristic frequency of the turbulence itself.

It represents the timescale of the turbulent response to the forcing of the mean flow. Looking again at equations (2.5) and (2.7), it is clear that the linear terms in these equations scale with the mean flow time scale S while the nonlinear terms, which include only fluctuating velocity, scale with the turbulent timescale ϵ/k. (For more details on the development of turbulence-to-mean-shear time scale ratio, see Tennekes and Lumley (1972).) Thus, $\frac{Sk}{\epsilon}$ is a ratio of the time scale of the mean flow production mechanism, S to that of the turbulent response $\frac{\epsilon}{k}$. In rapid distortion theory, we consider the limit in which the ratio $\frac{Sk}{\epsilon}$ is arbitrarily large, that is, the case where the distortions caused by the mean flow dominate. This implies that all terms in the above equations that scale with S also dominate, and in this limit, the nonlinear terms may be dropped. Thus, equations (2.5) and (2.7) simplify to

$$\frac{\overline{D}u_j}{\overline{D}t} = -u_i \frac{\partial \langle U_j \rangle}{\partial x_i} - \frac{1}{\rho}\frac{\partial p^{(r)}}{\partial x_j} \tag{2.12}$$

$$\frac{1}{\rho}\nabla^2 p^{(r)} = -2\frac{\partial \langle U_i \rangle}{\partial x_j}\frac{\partial u_j}{\partial x_i} \tag{2.13}$$

and these are called the *RDT equations*. Note that, in contrast to the full turbulence equations (Eqs. (2.5)and(2.7)), these equations are linear in the fluctuating velocity. This property makes them much easier to solve computationally. It is also interesting to note that in rapid distortion theory, the evolution of the velocity field depends solely on the amount of deformation and the geometry of deformation, rather than on the deformation rate (Pope, 2000).

B. Fourier Description of RDT

The observation in the previous section that the governing equations are linear in the fluctuating velocity leads to a simpler approach for treating RDT. This approach was first introduced by Taylor and Batchelor (1949). In this treatment, the turbulent

velocity field $\boldsymbol{u}(\boldsymbol{x},t)$ is represented by the sum of several Fourier modes. Keeping in mind that the RDT equations are linear in $\boldsymbol{u}$ and $p^{(r)}$ then it is clear that if $\boldsymbol{u}(\boldsymbol{x},t)$ is decomposed into Fourier modes, then each of these modes evolves independently. Further, the total number of Fourier modes remains constant, as the nonlinear cascade effect is absent. This treatment leads to the following type of assumed solution for the rapid-distortion equations:

$$\boldsymbol{u}(\boldsymbol{x},t) = \hat{\boldsymbol{u}}(t)e^{i\hat{\boldsymbol{\kappa}}(t)\cdot\boldsymbol{x}} \tag{2.14}$$

$$p^{(r)}(\boldsymbol{x},t) = \hat{p}(t)e^{i\hat{\boldsymbol{\kappa}}(t)\cdot\boldsymbol{x}} \tag{2.15}$$

where $\hat{\boldsymbol{\kappa}}(t)$ is the wavenumber vector and $\hat{\boldsymbol{u}}(t)$ is the Fourier coefficient. From these assumed solutions, it can be shown that the solution for $\boldsymbol{u}(\boldsymbol{x},t)$ above is determined by the following evolution equations for $\hat{\boldsymbol{\kappa}}(t)$ and $\hat{\boldsymbol{u}}(t)$(See Pope, 2000):

$$\frac{d\hat{\kappa}_l}{dt} = -\hat{\kappa}_j\frac{\partial\langle U_j\rangle}{\partial x_l} \tag{2.16}$$

$$\frac{d\hat{u}_j}{dt} = -\hat{u}_k\frac{\partial\langle U_l\rangle}{\partial x_k}\left(\delta_{jl} - 2\frac{\hat{\kappa}_j\hat{\kappa}_l}{\hat{\kappa}^2}\right). \tag{2.17}$$

These two equations govern the evolution of each Fourier mode in the turbulent velocity field $\boldsymbol{u}(\boldsymbol{x},t)$ in the RD limit. Note that these equations are further subject to the incompressibility condition (Pope, 2000)

$$\hat{u}_i\kappa_i = 0. \tag{2.18}$$

The wavenumber vector can also be decomposed as

$$\hat{\boldsymbol{\kappa}}(t) = \hat{\kappa}(t)\,\hat{\boldsymbol{e}}(t) \tag{2.19}$$

with the *unit wavevector* defined by

$$\hat{\boldsymbol{e}}(t) = \frac{\hat{\boldsymbol{\kappa}}(t)}{\hat{\kappa}(t)}. \tag{2.20}$$

From equation (2.17) we can see that the evolution of the Fourier coefficient does not depend on the magnitude of the wavenumber vector, but only its direction, and so equations (2.16) and (2.17) can be rewritten as follows:

$$\frac{d\hat{u}_j}{dt} = -\hat{u}_k \frac{\partial \langle U_l \rangle}{\partial x_k} (\delta_{jl} - 2\hat{e}_j \hat{e}_l) \tag{2.21}$$

$$\frac{d\hat{e}_l}{dt} = -\frac{\partial \langle U_m \rangle}{\partial x_i} \hat{e}_m (\delta_{il} - \hat{e}_i \hat{e}_l) \tag{2.22}$$

These equations completely describe the evolution of the turbulent velocity field $\hat{\boldsymbol{u}}(t)$. Again, these equations depend only on the unit wavevector for each wavenumber vector, that is, they depend only on the direction of each wave. In this way, the evolution of $\hat{\boldsymbol{e}}(t)$ given in equation (2.22) can be treated as a trajectory traced on a unit sphere. This treatment is used in the RDT calculations that are performed for the present study. (For more details in the above derivation, see Pope (2000).)

C. Spectral Description of RDT

The previous section developed the equations that govern the evolution of a single Fourier mode. This treatment can be generalized to consider a group of Fourier modes, which in turn can be generalized to represent a random fluctuating velocity field. In this manner, we can consider a fluctuating velocity field $\boldsymbol{u}(\boldsymbol{x}, t)$, with an initial condition given by:

$$\boldsymbol{u}(\boldsymbol{x}, 0) = \sum_{\boldsymbol{\kappa}^\circ} e^{i\boldsymbol{\kappa}^\circ \cdot \boldsymbol{x}} \, \hat{\boldsymbol{u}}(\boldsymbol{\kappa}^\circ, 0) \tag{2.23}$$

where $\boldsymbol{\kappa}^\circ = \boldsymbol{\kappa}(t=0)$ is a set of initial wavenumbers and $\hat{\boldsymbol{u}}(\boldsymbol{\kappa}^\circ, 0)$ is the Fourier coefficient associated with these wavenumbers. Again we point out that as the velocity field evolves according to the RDT equations (Eqs. (2.16 and (2.17)), the number of waves in the flow field remain the same as a consequence of the linearity of the equations. However, the wavenumbers (or wavelengths) and the amplitude of each of these waves will evolve. Thus, at any later time, each wave present in the flow can be identified according to either its initial wavenumber $\boldsymbol{\kappa}^\circ$ or its current value $\hat{\boldsymbol{\kappa}}(t)$. In this way, the velocity field at any subsequent time can be given by

$$\boldsymbol{u}(\boldsymbol{x}, t) = \sum_{\boldsymbol{\kappa}^0} e^{i\hat{\boldsymbol{\kappa}}\cdot\boldsymbol{x}}\, \hat{\boldsymbol{u}}(\boldsymbol{\kappa}^\circ, t) \tag{2.24}$$

At this point, we introduce a quantity called the *velocity-spectrum tensor*, $\Phi_{ij}(\boldsymbol{\kappa}, t)$ which gives a statistical representation of the turbulent velocity field:

$$\Phi_{ij}(\boldsymbol{\kappa}, t) = \Big\langle \sum_{\boldsymbol{\kappa}^\circ} \delta(\boldsymbol{\kappa} - \hat{\boldsymbol{\kappa}}(t)) \hat{u}_i^*(\boldsymbol{\kappa}^\circ, t)\; \hat{u}_j(\boldsymbol{\kappa}^\circ, t) \Big\rangle. \tag{2.25}$$

The velocity spectrum tensor represents the contribution of the Fourier mode $e^{i\boldsymbol{\kappa}\cdot\boldsymbol{x}}$ to the Reynolds stress $\langle u_i u_j \rangle$. Thus it can be viewed as the Reynolds stress density in wavenumber space. The above definition is for the velocity spectrum tensor when it is parameterized by the current wavenumber $\hat{\boldsymbol{\kappa}}(t)$. The velocity spectrum tensor parameterized the initial wavenumber $\boldsymbol{\kappa}^\circ$ is expressed as

$$\Phi_{ij}^\circ(\boldsymbol{\kappa}, t) = \Big\langle \sum_{\boldsymbol{\kappa}^\circ} \delta(\boldsymbol{\kappa} - \boldsymbol{\kappa}^\circ) \hat{u}_i^*(\boldsymbol{\kappa}^\circ, t) \hat{u}_j(\boldsymbol{\kappa}^\circ, t) \Big\rangle. \tag{2.26}$$

Since the velocity-spectrum tensor represents the Reynolds-stress density in wavenumber space, Φ_{ij} can be integrated over all wavenumbers to obtain the Reynolds stress, given by

$$\langle u_i u_j \rangle = \iiint_{-\infty}^{\infty} \Phi_{ij}(\boldsymbol{\kappa}, t)\; d\boldsymbol{\kappa} = \Big\langle \sum_{\boldsymbol{\kappa}^\circ} \hat{u}_i^*(\boldsymbol{\kappa}^\circ, t)\; \hat{u}_j(\boldsymbol{\kappa}^\circ, t) \Big\rangle. \tag{2.27}$$

Using the above definition of the velocity-spectrum tensor (Eq.(2.25)) and keeping in mind the evolution equations for $\hat{\boldsymbol{\kappa}}(t)$ and $\hat{\boldsymbol{u}}(t)$ (Eqs.(2.16) and (2.17)), the equation for the evolution of the velocity-spectrum tensor can be derived as

$$\frac{\partial \Phi_{ij}}{\partial t} = \frac{\partial \langle U_m \rangle}{\partial x_l} \kappa_m \frac{\partial \Phi_{ij}}{\partial \kappa_l} - \frac{\partial \langle U_i \rangle}{\partial x_k} \Phi_{kj} - \frac{\partial \langle U_j \rangle}{\partial x_k} \Phi_{ik} + 2 \frac{\partial \langle U_l \rangle}{\partial x_k} \Big(\frac{\kappa_i \kappa_l}{\kappa^2} \Phi_{kj} + \frac{\kappa_j \kappa_l}{\kappa^2} \Phi_{ik} \Big). \quad (2.28)$$

This equation gives the evolution of a turbulence spectrum in the rapid distortion limit. For future considerations is is useful to note the physical significance of the different terms on the right hand side of this equation. The first term represents the transport of the turbulent spectrum in wavenumber space. The next two terms represent turbulent production, and the last terms represent the rapid pressure-strain correlation. The evolution equation for the spectrum parameterized by the initial wavenumber can also be derived and is given by

$$\frac{\partial \Phi^{\circ}_{ij}}{\partial t} = - \frac{\partial \langle U_i \rangle}{\partial x_k} \Phi^{\circ}_{kj} - \frac{\partial \langle U_j \rangle}{\partial x_k} \Phi^{\circ}_{ik} + 2 \frac{\partial \langle U_l \rangle}{\partial x_k} \Big(\frac{\kappa_i \kappa_l}{\kappa^2} \Phi^{\circ}_{kj} + \frac{\kappa_j \kappa_l}{\kappa^2} \Phi^{\circ}_{ik} \Big). \quad (2.29)$$

Note this equation is the same as equation (2.28) except for the omission of the transport term. Thus, in this equation the first two terms represent production and the last terms represent rapid pressure.

a. RDT Reynolds Stress Equation

Now, just as with the equation for the velocity-spectrum tensor itself, we can integrate the evolution equation for the velocity-spectrum tensor (Eq.(2.28)) over all wavenumbers to obtain an evolution equation for the Reynolds stress in the RD limit:

$$\frac{\partial}{\partial t} \langle u_i u_j \rangle = - \langle u_j u_k \rangle \frac{\partial \langle U_i \rangle}{\partial x_k} - \langle u_i u_k \rangle \frac{\partial \langle U_j \rangle}{\partial x_k} + 2 \frac{\partial \langle U_l \rangle}{\partial x_k} (M_{kjil} + M_{ikjl}) \quad (2.30)$$

where M_{ijkl} is a fourth order tensor defined by

$$M_{ijkl} = \iiint_{-\infty}^{\infty} \Phi_{ij} \frac{\kappa_k \kappa_l}{\kappa^2} d\boldsymbol{\kappa} = \sum_{\underline{\kappa}^\circ} \hat{u}_i^* \hat{u}_j \frac{\hat{\kappa}_k \hat{\kappa}_l}{\hat{\kappa}^2} = \sum_{\underline{\kappa}^\circ} \hat{u}_i^* \hat{u}_j \hat{e}_k \hat{e}_l. \tag{2.31}$$

If we define the production, P_{ij} as

$$P_{ij} = -\langle u_j u_k \rangle \frac{\partial \langle U_i \rangle}{\partial x_k} - \langle u_i u_k \rangle \frac{\partial \langle U_j \rangle}{\partial x_k} \tag{2.32}$$

and the rapid pressure-rate-of-strain tensor $R_{ij}^{(r)}$ as

$$R_{ij}^{(r)} = 2 \frac{\partial \langle U_l \rangle}{\partial x_k} (M_{kjil} + M_{ikjl}), \tag{2.33}$$

we can rewrite equation (2.30) as

$$\frac{\partial}{\partial t} \langle u_i u_j \rangle = P_{ij} + R_{ij}^{(r)}. \tag{2.34}$$

For more details in this development of RDT theory, see Pope (2000).

b. Inertial Model

The rapid distortion limit considers the physics of inertial (production) and rapid pressure effects. Further simplification can be made to isolate the contributions of each effect. Towards this end, we can also consider the case where the rapid-pressure term is omitted, this we call the *Inertial Model*. In the Inertial Model for RDT, the evolution of the velocity field is governed only by inertial action. Thus, the evolution equation for the velocity-spectrum tensor for the Inertial Model becomes

$$\frac{\partial \Phi_{ij}^\circ}{\partial t} = 2 \frac{\partial \langle U_l \rangle}{\partial x_k} \Big(\frac{\kappa_i \kappa_l}{\kappa^2} \Phi_{kj}^\circ + \frac{\kappa_j \kappa_l}{\kappa^2} \Phi_{ik}^\circ \Big). \tag{2.35}$$

Just as with the full Reynolds Stress Equation, we can integrate this evolution equation over all wavenumbers to obtain the Reynolds stress evolution equation for the

Inertial Model:

$$\frac{\partial}{\partial t}\langle u_i u_j\rangle = -\langle u_j u_k\rangle \frac{\partial\langle U_i\rangle}{\partial x_k} - \langle u_i u_k\rangle \frac{\partial\langle U_j\rangle}{\partial x_k} \tag{2.36}$$

or

$$\frac{\partial}{\partial t}\langle u_i u_j\rangle = P_{ij}. \tag{2.37}$$

This is the Inertial Model Reynolds stress equation. Again, this model is similar to RDT, but it differs in the fact that it considers inertial effect only, and omits the effect of the rapid pressure. Although the Inertial Model velocity field does not satisfy the incompressibility condition, it can provide important insight into the turbulence process.

These equations form the theoretical basis for the computer implementation of RDT for the present work, and its application to the study of unsteadily-forced turbulence. Throughout this thesis, we will compare RDT results with Inertial Model Results to identify the effects of the rapid pressure physics.

CHAPTER III

RDT SIMULATIONS

In this section, the numerical implementation of the above RDT equations and the details of the calculations that were performed are presented. The RDT equations are solved using a fourth order Runge-Kutta solution scheme. The implementation consists of three main parts, each of which is outlined below. First, the turbulent velocity field is initialized by defining a set of wavenumbers that correspond to an isotropic initial condition. Next, the simulation itself is performed which solves the appropriate evolution equations using the fourth order Runge-Kutta scheme. Finally, from the raw RDT data, other relevant physical parameters in the flow are calculated. Much of the code development is similar to that presented in Girimaji, Jeong and Poroseva (2003).

A. Initialization

The first step in performing the RDT simulation is to initialize the turbulent velocity field. In the present study, we consider an initially isotropic velocity field that is subsequently subjected to unsteady forcing. Recalling the Fourier description of RDT in the previous chapter, it can be seen that this initially isotropic velocity field corresponds to a set of wavenumber vectors that are evenly distributed over a unit sphere in wavenumber space. For a perfectly accurate calculation we would need an infinite number of wavenumber vectors distributed over the sphere. Naturally this is not computationally feasible. In the program that has been implemented for the present study, the number of points defined on the surface of the sphere is defined by a parameter N_ϕ. Specifically N_ϕ indicates the number of equally distributed points that are to be defined on a unit half circle on the wavenumber sphere. This number

is then used to generate the points over the entire unit sphere that correspond to the density given by N_ϕ for the half circle. (For more details, see Girimaji, Jeong and Poroseva (2003).

In the present study, all calculations have been made with an N_ϕ value of 50, which corresponds to the generation of approximately 6000 points for wavenumber vectors that are distributed evenly over the unit sphere. Once the locations of the points on the unit sphere are defined for an isotropic initial condition, the wavenumber vectors themselves are defined. Here we assume that the turbulent kinetic energy is evenly distributed with respect to the wavenumber vectors, and therefore the magnitude of each wavenumber vector is initialized to unity. Before proceeding to the calculations, the spectrum is checked to assure that it satisfies continuity, a condition defined by

$$\kappa_i \langle u_i u_j \rangle = \kappa_j \langle u_i u_j \rangle = 0. \tag{3.1}$$

B. Simulation

Once the isotropic set of wavenumber vectors is initialized, the calculations for the evolution of the turbulent velocity field can be made. The program uses a fourth order Runge-Kutta scheme to find the solution to the RDT evolution equations at each time step. The equations that are solved for the full RDT case are equation (2.16) for the wavenumber evolution and equation (2.29) for the evolution of the Reynolds stresses conditioned on a given wavenumber. Calculations are also made for the velocity field evolution for the Inertial Model case. In this case, the same wavenumber evolution equation is used, while the Reynolds stress evolution equation used in the calculations is equation (2.36).

One of the most important features of the solution procedure is the treatment

of the time-dependent mean velocity gradient tensor. Since the present study is concerned with the turbulent response to unsteady forcing, the role of the velocity gradient tensor, $\frac{\partial U_i}{\partial x_j}$ in the calculations is a central one. This consideration is discussed in the following section.

C. Characterization of Forcing

The study of homogeneous shear turbulence has been central to our understanding of constantly (time-independently) forced turbulence. Therefore, it is natural that our study of unsteadily-forced turbulence be centered around an unsteady analog of constant homogeneous turbulence. The mean velocity field used in this study corresponds to a flow in which the shear is rotating. In other words, the eigen-directions of the shear tensors rotate uniformly while the eigenvalues remain constant. This flow is quite distinct from homogeneous shear flow in a rotating reference frame. To incorporate this unsteady forcing into the simulations, we define two sinusoidal forcing functions:

$$f_1 = sin(2\pi\Lambda t) \tag{3.2}$$

and

$$f_2 = cos(2\pi\Lambda t). \tag{3.3}$$

In these equations, Λ is the dimensional forcing frequency. We report the results in terms of a nondimensional frequency λ given by

$$\lambda = \Lambda/S. \tag{3.4}$$

In the present calculations, S is always unity, and so $\lambda = \Lambda$. Due to this fact, we will use λ and Λ synonymously through this thesis.

The time-dependent velocity gradient tensor for our study, then, is defined as:

$$\begin{aligned}\frac{\partial U_i}{\partial x_j} &= \begin{pmatrix} f_1 f_2 & f_2 f_2 & 0 \\ -f_1 f_1 & -f_1 f_2 & 0 \\ 0 & 0 & 0 \end{pmatrix} \\ &= \begin{pmatrix} sin(2\pi\lambda t)cos(2\pi\lambda t) & cos^2(2\pi\lambda t) & 0 \\ -sin^2(2\pi\lambda t) & -sin(2\pi\lambda t)cos(2\pi\lambda t) & 0 \\ 0 & 0 & 0 \end{pmatrix}\end{aligned} \tag{3.5}$$

This velocity gradient tensor represents time-dependent but homogeneous oscillatory motion. The forcing frequency is defined for a given calculation by a specification of λ, and held constant for the duration of that calculation. When $\lambda = 0$, this velocity gradient tensor reduces to

$$\frac{\partial U_i}{\partial x_j} = \begin{pmatrix} 0 & 1 & 0 \\ 0 & 0 & 0 \\ 0 & 0 & 0 \end{pmatrix} \tag{3.6}$$

which is a steady homogeneous shear flow case. Thus, the current study considers the oscillating shear case where $\overline{S}(t) = \sqrt{S_{ij}(t)S_{ij}(t)} = const.$ During the solution process, the time-dependent velocity gradient tensor is updated at each timestep during the solution. This includes the appropriate temporal updating at each individual step of the Runge-Kutta process.

Initially, values for λ were chosen to cover a broad range of forcing frequencies. When different physical responses of the turbulence to the different forcing frequencies began to emerge, the frequencies of interest were narrowed down and chosen to better examine and differentiate between the physical phenomena that had become evident. Table I shows the forcing frequencies used in the present study. Note that the frequencies in bold are the primary ones that are used for the reporting of the

results in Chapter IV. Calculations were made for both the Inertial Model and the full

Table I. Forcing Frequencies

Regime	λ
Zero Frequency	**0.00**
Low Frequency	**0.02** 0.04 0.06 **0.08** 0.10 0.12 **0.14**
Intermediate Frequency	**0.16** **0.18** 0.20
High Frequency	**0.30** 0.40 **0.50**

RDT case at these frequencies. The Runge-Kutta solution of the evolution equations results in evolution data for the wavenumbers and the Reynolds stresses.

D. Calculation of Statistics

The final step in the calculation process is the computation of the other relevant statistical values in the turbulent field. Once the data for the evolution for the wavenumbers, the Reynolds stresses, and the mean velocity gradients have been calculated by the Runge-Kutta calculation, the evolution data for other statistics can be computed from these. These include, but are not limited to the production:

$$P_{ij} = -\langle u_j u_k \rangle \frac{\partial \langle U_i \rangle}{\partial x_k} - \langle u_i u_k \rangle \frac{\partial \langle U_j \rangle}{\partial x_k}, \tag{3.7}$$

the rapid pressure-strain correlation:

$$R_{ij}^{(r)} = 2\frac{\partial\langle U_l\rangle}{\partial x_k}(M_{kjil} + M_{ikjl}), \tag{3.8}$$

the turbulent kinetic energy:

$$k = \frac{1}{2}\langle u_i u_i\rangle, \tag{3.9}$$

and the components of the Reynolds stress anisotropy tensor

$$b_{ij} = \frac{\langle u_i u_j\rangle}{2k} - \frac{1}{3}\delta_{ij}; \tag{3.10}$$

where δ_{ij} is the *Kronecker delta* defined by

$$\delta_{ij} = \begin{cases} 0 & i \neq j \\ 1 & i = j \end{cases}. \tag{3.11}$$

These calculated statistics, along with the original evolution data for the Reynolds stresses and the unsteady velocity gradient tensor form the complete set of RDT and Inertial Model data that is presented in this thesis.

CHAPTER IV

RESULTS

Results from the RDT calculations for unsteadily-forced turbulence are presented in this chapter. The RDT calculations were implemented as described in Chapter III, and computations were made for forcing frequencies specified in Table I to observe the physical response of the turbulent field to the different frequencies. These calculations provided data for the evolution of the turbulent kinetic energy, Reynolds-stress anisotropy, turbulent production, and rapid pressure-strain correlation. The calculations were performed first using the Inertial Model to observe the evolution of the turbulent field in the absence of rapid pressure effects. Next, the same set of forcing frequencies was considered in calculations using full RDT, including the rapid pressure term.

Since the Inertial Model omits the effects of rapid-pressure (see Eq.(2.36)), it essentially describes the effects of the production mechanism, that is, the applied distortion, in the turbulent field without any consideration of the response of the turbulence itself. Previous work has already considered the problem of turbulence subjected to steady homogeneous shear distortion in the rapid distortion limit (see the discussion in Chapter I). A brief look at the response of an initially isotropic turbulent velocity field when it is subjected to a constant homogeneous shear distortion (see Eq.(3.6)) for both the Inertial Model case and for full RDT can give some insight into why it might be useful to consider both cases for the present study. Figure 1 shows the evolution of the b_{11}, b_{22}, and b_{12} components of the Reynolds stress anisotropy tensor for homogeneous shear distortion for both the Inertial Model and RDT.

From the figure it is clear that at early times there is a quantitative difference between the predictions of the Inertial Model and those of RDT for homogeneous

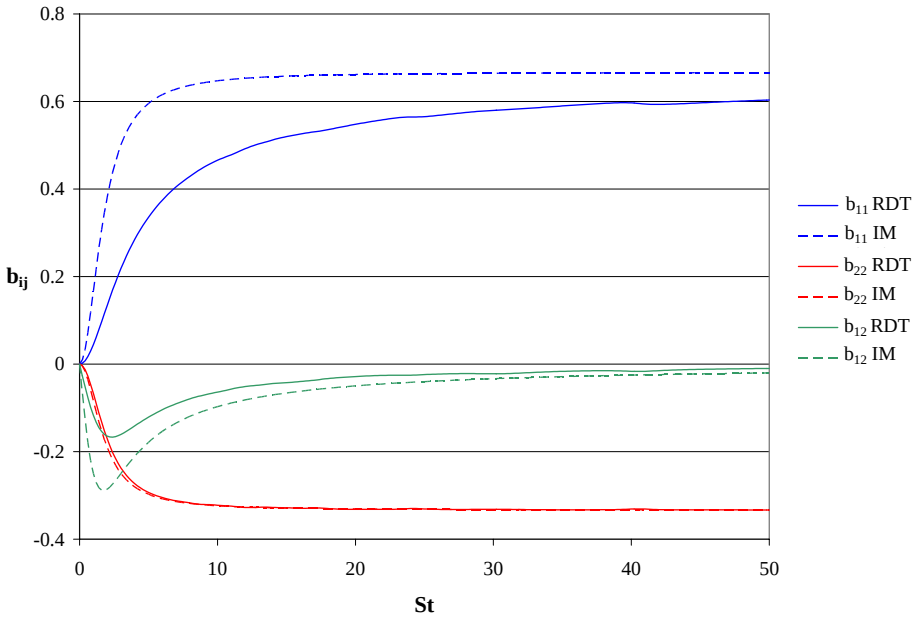

Fig. 1. Inertial Model vs. RDT for Homogeneous Shear ($\lambda = 0$)

shear distortion. This is evident for the b_{11} and b_{12} components. At early times, these components exhibit steep gradients for the Inertial Model calculation, while the RDT results show an early behavior that can be characterized as somewhat damped. However, while there are some quantitative differences, it seems that the Inertial Model predicts the qualitative features quite well. The qualitative differences illustrate the activity of the rapid pressure in the turbulent field and indicate that the rapid pressure serves to counteract the production mechanism in homogeneous shear rapid distortion. (According to theory, in initially isotropic turbulence, the rapid pressure counteracts 60% of the production in homogeneous shear flow. For more details, see Pope (2000)) Since the Inertial Model and RDT results appear to converge a later times, and it can be inferred from this fact that the Inertial Model actually sets the asymptotic behavior of the RDT solutions.

While the roles of the production and rapid pressure are relatively well under-

stood for the constant homogeneous shear distortion case above, the present study considers the case of periodically-forced homogeneous distortion, a situation not previously considered in detail. For this case, then, we also consider both the Inertial Model and full RDT. In a manner similar to the homogeneous shear case, it is expected that the Inertial Model should give some qualitative insight into the changes in the initially isotropic velocity field due to the periodic forcing. In addition, just as in the homogeneous shear case above, any differences between the behaviors predicted by the Inertial Model and full RDT will illustrate the effect of the rapid pressure, that is, the influence of the straining response of the turbulent field due to the applied distortion.

The results themselves are presented in two main sections. In the first section, results from the Inertial Model calculations are given. These include the evolution turbulent kinetic energy, and components of the Reynolds stress anisotropy tensor as well as production for several different forcing frequencies. Obviously, all components of the rapid pressure-strain correlation in the Inertial Model case are zero. In the second section, the full RDT calculation results are presented. The results in this section include data for the same parameters given for the Inertial Model case, as well data for the evolution of the rapid pressure-strain correlation.

A. Inertial Model Results

In this section, the results for the calculations performed for unsteadily-forced turbulence using the Inertial Model are presented. Inertial model simulations were performed for the range of forcing frequencies previously presented in Table I. The results are presented in the form of plots of the evolution over time of the various turbulent flow parameters that are considered. These include the turbulent kinetic

energy, Reynolds-stress anisotropy and turbulent production. For all cases, the initial turbulent velocity is isotropic, and the applied distortion is that given previously in equation (3.5).

1. Turbulent Kinetic Energy

The first parameter to be considered in the Inertial Model case is the turbulent kinetic energy. The results for the evolution of the kinetic energy for a periodically-forced turbulent velocity field in the rapid distortion limit are shown in Figures 2-4. In

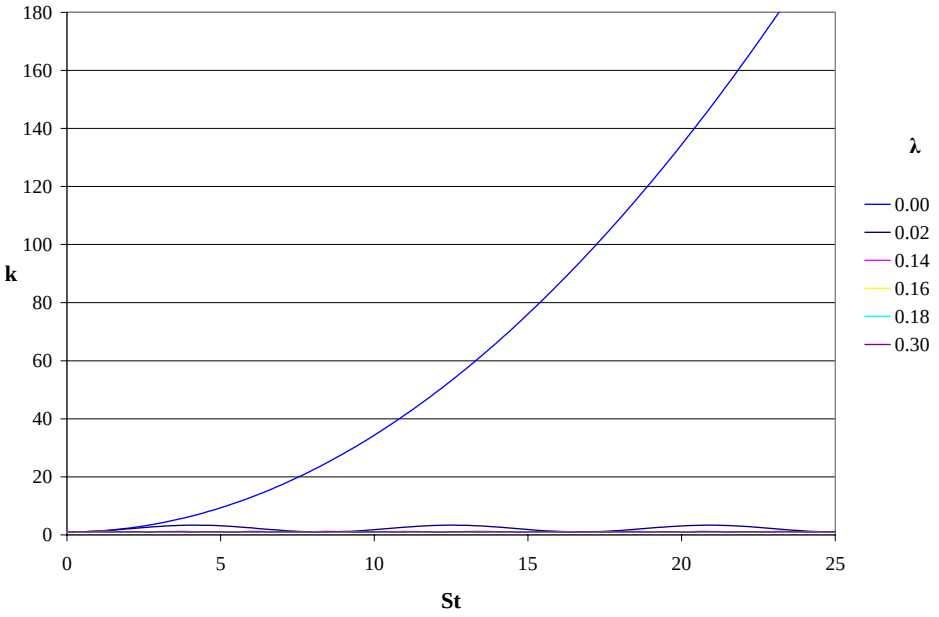

Fig. 2. Inertial Model - Kinetic Energy Evolution (Large Scale)

the figures, the case of zero forcing frequency corresponds to a homogeneous shear distortion applied to the velocity field. For this case, the turbulent kinetic energy, as expected, exhibits a monotonic increasing behavior, a result noted previously. In addition, the slope of the turbulent kinetic evolution for the homogeneous shear case appears to be increasing steadily. This behavior is in agreement with the Inertial

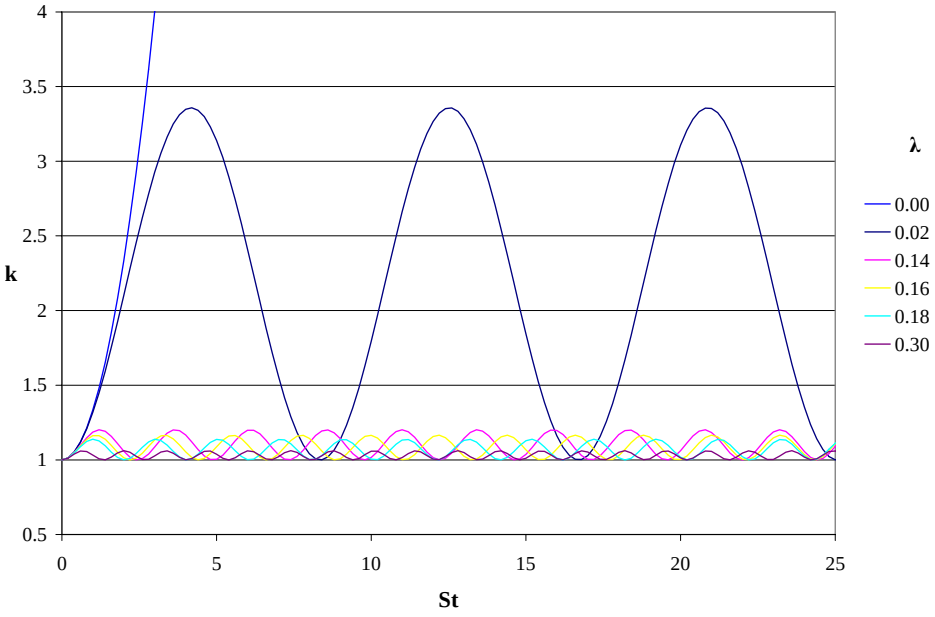

Fig. 3. Inertial Model - Kinetic Energy Evolution (Medium Scale)

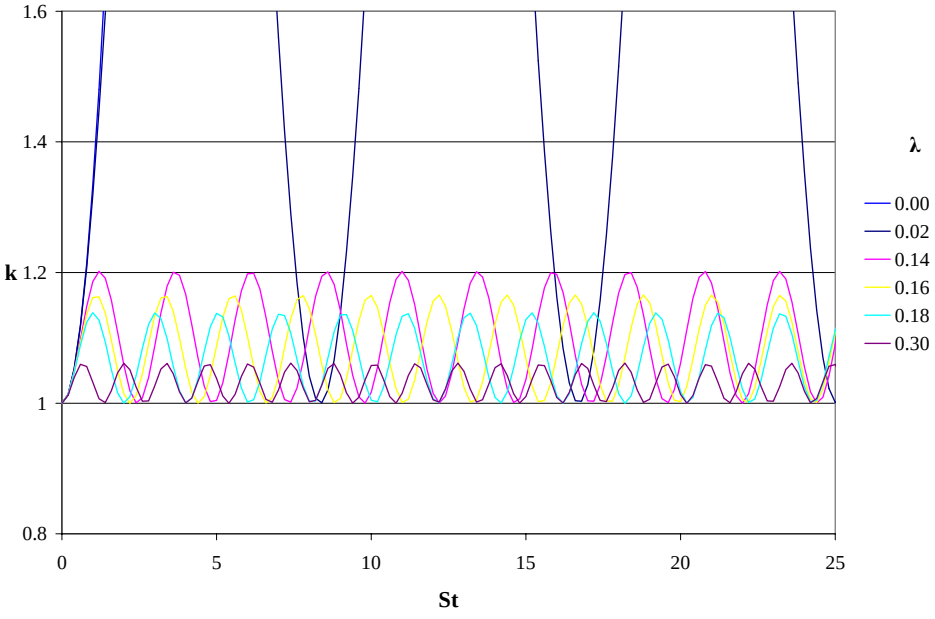

Fig. 4. Inertial Model - Kinetic Energy Evolution (Small Scale)

Model equation for the evolution of the Reynolds stresses (Eq.(2.36)). This equation stipulates that the gradients of the Reynolds stresses are directly dependent upon the production. In homogeneous shear distortion, the production increases linearly, and this leads to the observed behavior in which the slope of the kinetic energy evolution equation increases linearly as well.

Next, we consider the cases where the periodic forcing of the turbulent velocity field is present. For all the nonzero forcing frequencies shown, the evolution of the turbulent kinetic energy exhibits pure periodicity. The oscillatory behavior for each case is bounded by its initial value of unity (for all cases) as a minimum, and with with a maximum that decreases with increasing forcing frequency. It has already been observed (See Chapter II) that that the calculations of the Inertial Model illustrate the role of the production mechanism, and so it is expected that in the case of periodic forcing, the evolution of the kinetic energy is also periodic in nature. Therefore the above result is an expected one, and, as stated above, it is expected that this result also gives some qualitative feel for the actual response of the turbulent field for periodic forcing. Finally, it is useful to also note that for this Inertial Model case, the evolution of turbulent kinetic energy exhibits no dissipative effects, and so for a velocity field under unsteady forcing, the process is fully reversible.

2. Reynolds Stress Anisotropy

The evolution of components of the Reynolds Stress Anisotropy tensor for Inertial Model is considered next. The components of the Reynolds Stress Anisotropy tensor at each moment give information as to the relative isotropy of the velocity field. Since the initial condition for the velocity field is isotropic (see Chapter III), the evolution of the b_{11}, b_{22}, and b_{12} components that are given below have initial values of zero. Figures 5-10 below show the evolution of the different components of the

Reynolds stress anisotropy tensor for periodically-forced turbulent flow in the rapid distortion limit, as predicted by the Inertial Model. In the figures, we again look first at the homogeneous shear distortion case ($\lambda = 0$). Note that evolution of the b_{11} and b_{22} components clearly converge to values of 2/3 and -1/3, respectively, while the b_{12} component converges slowly to zero. If we recall the definition of b_{ij} given in equation (3.10), it is clear that these are the appropriate values for the convergence of these components of the anisotropy tensor as the flow approaches the one-component limit, as is the case for constant homogeneous shear distortion. Thus, as expected, the Inertial Model directly illustrates the role of the production mechanism as the components of the Reynolds-stress anisotropy tensor converge to values that directly correspond to those associated with the type of subjected distortion.

Next we consider the cases in the figures where the periodic forcing of the turbulent velocity field is present. The results show a behavior that is somewhat analogous to the results for the evolution of the turbulent kinetic energy. Again for the nonzero forcing cases, we see a regular periodic evolution for all three components, although the oscillations are clearly more complex than in those for kinetic energy. Recall that the kinetic energy evolution is directly dependent on the production specifically, which has pure single-mode oscillations according to the applied periodic distortion, and hence simple oscillatory behavior is expected for the kinetic energy evolution. Of course, since we are presently considering the Inertial Model, the evolution of the Reynolds-stress anisotropy is also dependent on the production, but its dependence is not as direct as that of the kinetic energy. Specifically, the Reynolds stresses are have two contributions which determine its evolution, and while these contributions both depend directly on the production, their combined effect on the Reynolds stress anisotropy leads to an evolution that is not simple, but rather contains more than one mode. Looking again at the equation for the Reynolds-stress anisotropy components

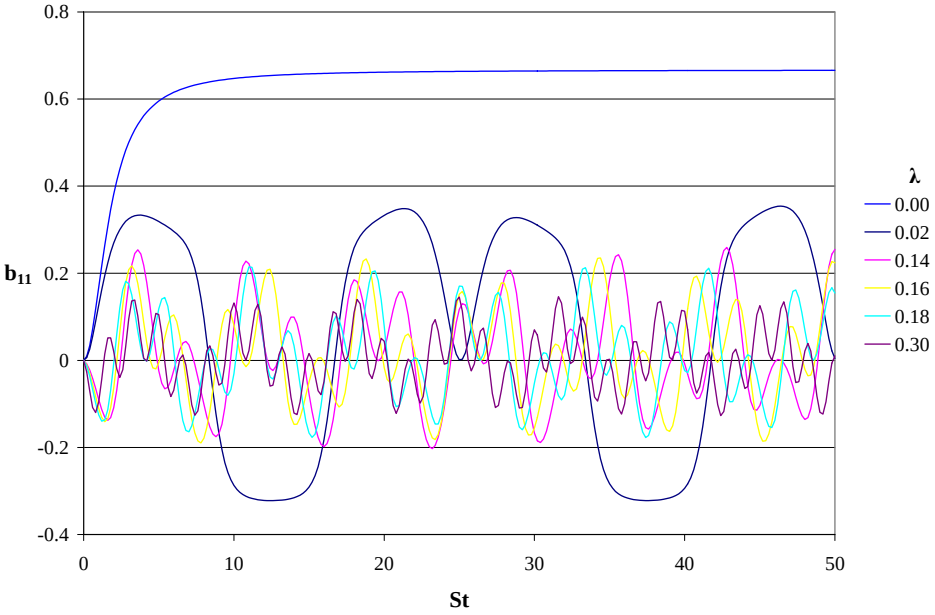

Fig. 5. Inertial Model - b_{11} Evolution (Full View)

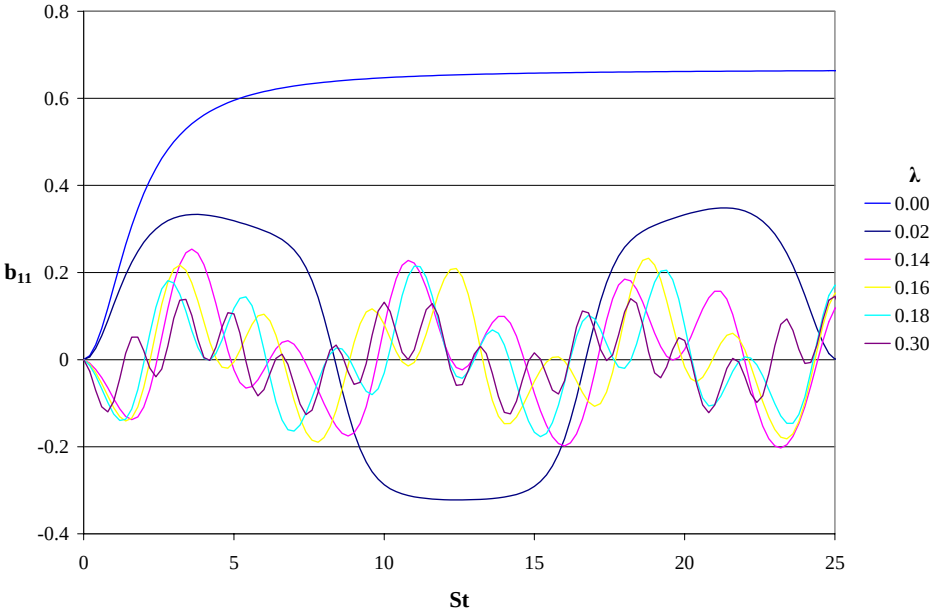

Fig. 6. Inertial Model - b_{11} Evolution (Close-up View)

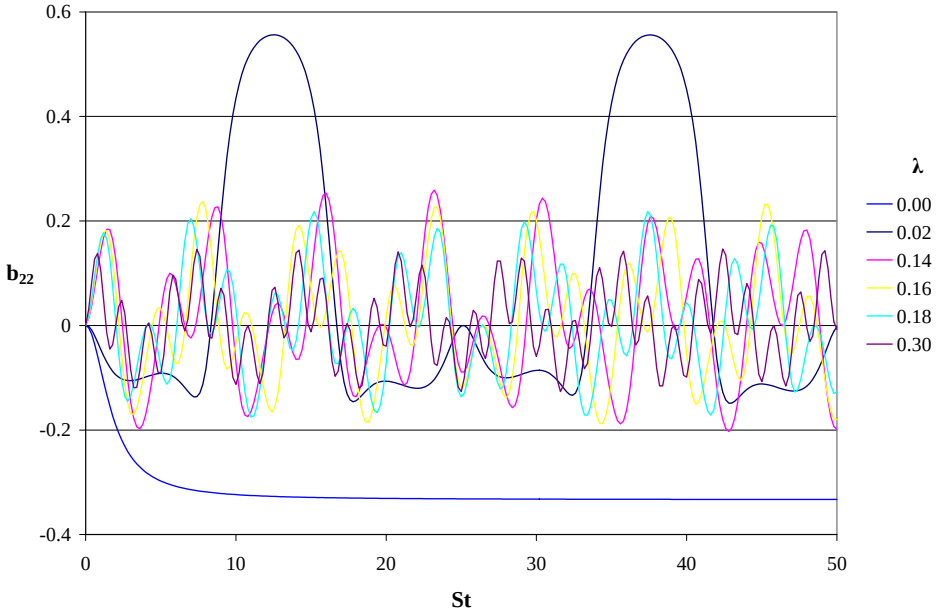

Fig. 7. Inertial Model - b_{22} Evolution (Full View)

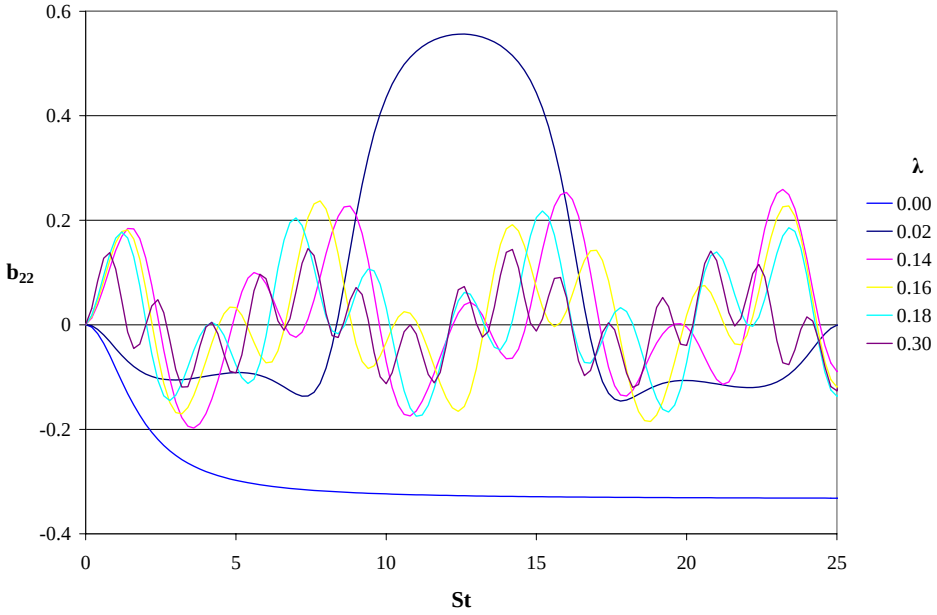

Fig. 8. Inertial Model - b_{22} Evolution (Close-up View)

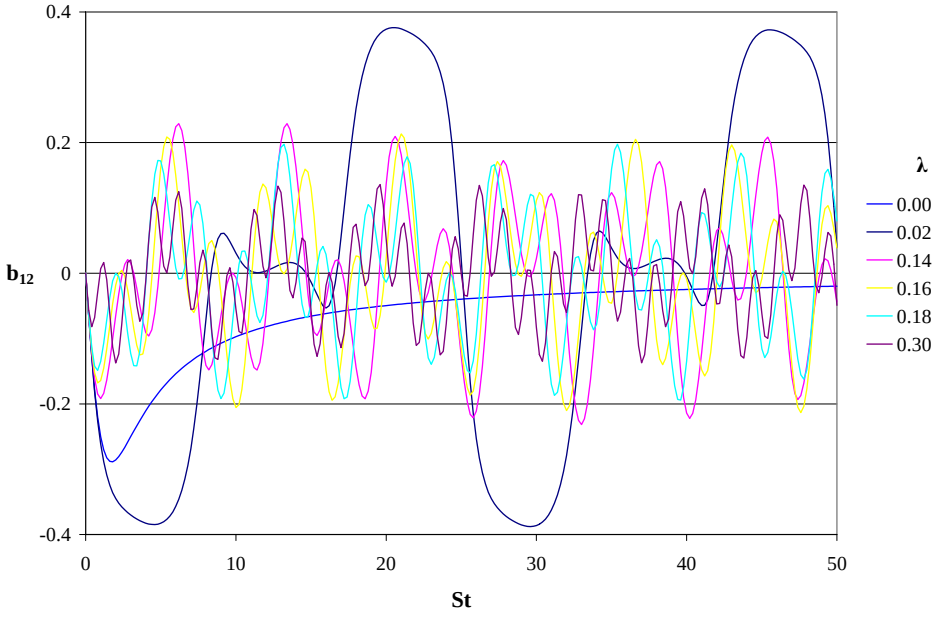

Fig. 9. Inertial Model - b_{12} Evolution (Full View)

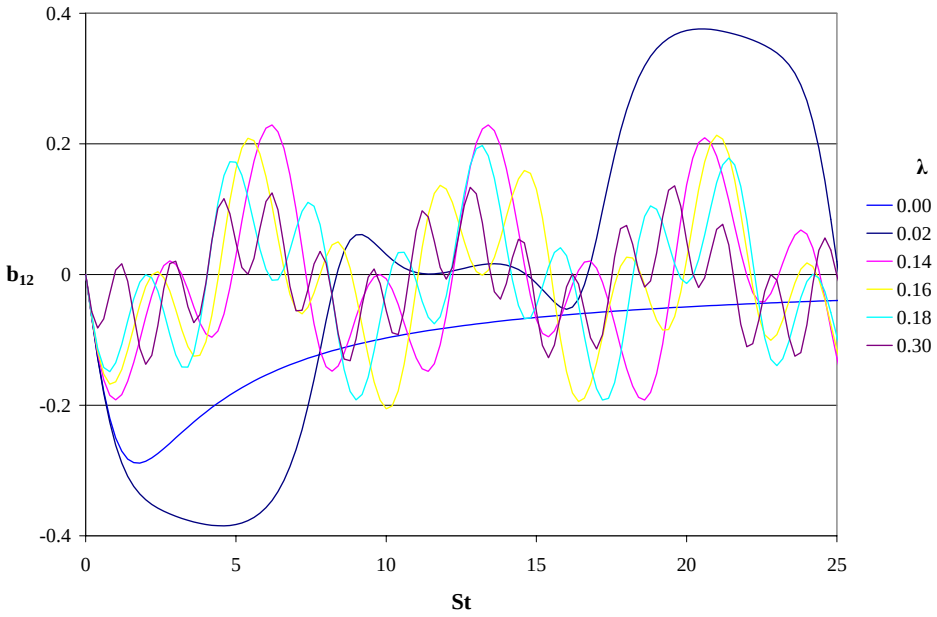

Fig. 10. Inertial Model - b_{12} Evolution (Close-up View)

(Eq.(3.10)) it can be seen that the evolution of this parameter depends not only on the evolution of the Reynolds stress (which, in turn is directly dependent on production), but also on the evolution of the kinetic energy (which is also, in turn, directly dependent on production). The influence of these two parameters yields the complex oscillatory motion seen for all three components shown in the figures.

3. Turbulent Production

Finally, the evolution of the turbulent production for the Inertial Model is considered. The evolution behavior given in the figures can be helpful in understanding the role of production in the evolution of the turbulent kinetic energy and Reynolds stress anisotropy, as discussed above. Figures 11 and 12 below show the evolution of the P_{11} component of production, normalized by the kinetic energy. Again, note first

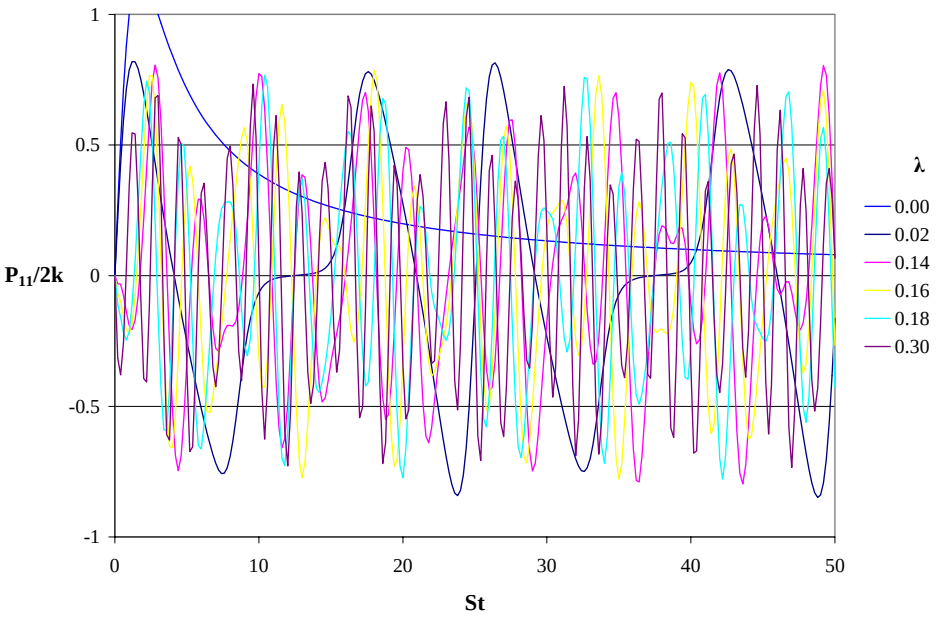

Fig. 11. Inertial Model - Evolution of Production (Full View)

the zero frequency homogeneous shear distortion case. For this case, the evolution of

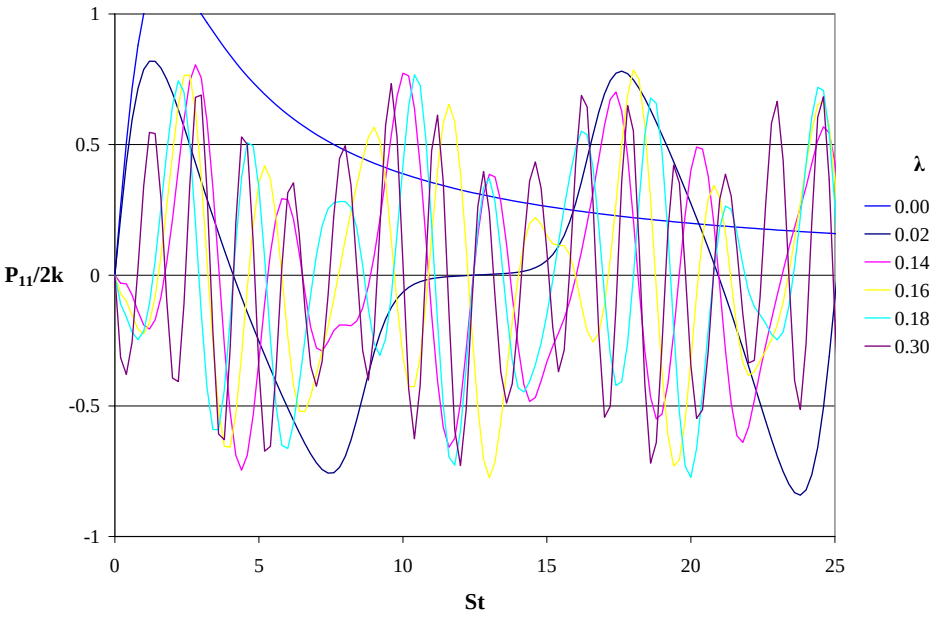

Fig. 12. Inertial Model - Evolution of Production (Close-up View)

the normalized P_{11} increases initially, and at very early times this increase appears to be nearly linear. The growth levels off, however, as the production begins to decrease with an apparent tendency to converge to a value of zero. We know that for a velocity field subjected to steady homogeneous shear distortion in the rapid distortion limit, the production increases linearly. It has also been shown above that the kinetic energy increases without bound for this distortion case. So both the early linear increase and the long-term tendency for $P_{11}/2k$ to converge to zero are expected for the homogeneous shear case.

Once again, we next consider the cases with periodic forcing. As with the evolution of the Reynolds stress anisotropies, we see oscillatory evolution for the production that clearly is made up of several modes. In the case of the anisotropy tensor, these modes were due to the contribution of two separate terms. Looking again at the definition of production (Eq.(2.32)), it is clear that the evolution is dependent on both

the Reynolds stresses and the applied velocity gradient. Thus, as with the anisotropy evolution, it is the influence of these two parameters that determines the oscillatory evolution for P_{11} that is shown in the figures. Overall, however, it is important to note (as will be seen in subsequent sections) that the evolution of the production, and indeed of all the above parameters is 'well behaved'. That is, the Inertial Model dictates that for periodically-forced homogeneous turbulence, the evolutions of all parameters exhibit regular oscillatory response that is bounded.

B. Full RDT Results

In this section, the results for the calculations performed for periodically-forced turbulence using the the full Rapid Distortion Equations (equations (2.16) and (2.30)) are presented. The full RDT calculations were performed for the same set of frequencies as those made for the Inertial Model above (see Table I), and the results are also presented for the same select reported forcing frequencies. Again, the results are presented in the form of plots of the evolution over time of the various turbulent flow parameters that are considered. As previously discussed, RDT contrasts with the Inertial Model in that it also includes the effect of rapid pressure. We have already seen the behavior of the production mechanism acting alone in the Inertial Model results in the previous section. In the results presented in this section we also see the effects of the response of the turbulent velocity field due to this production mechanism.

Therefore, as with the Inertial Model, the data for the evolution of the kinetic energy, Reynolds-stress anisotropy, and turbulent production for the case of periodically-forced turbulence are presented here for the full RDT case. In addition, the full RDT results for the evolution of the rapid pressure-strain correlation are also presented here. As before, the turbulent velocity field is initialized to be isotropic and the

applied periodic forcing is given by equation (3.5) for the time-dependent velocity gradient tensor that is considered in this study.

The results in this section can be examined and compared to the Inertial Model results already presented, and any differences in behavior can can be attributed to the presence of the rapid pressure-strain correlation term, which distinguishes full RDT from the Inertial Model.

1. Turbulent Kinetic Energy

The first parameter presented here for the full RDT case is the turbulent kinetic energy. Results for the evolution of the kinetic energy for a periodically-forced turbulent velocity field in the rapid distortion limit are shown in figures 13-16. Figure 13 below shows the complete RDT results for all forcing frequencies calculated in this study, and for an extended time. This figure immediately illustrates a very im-

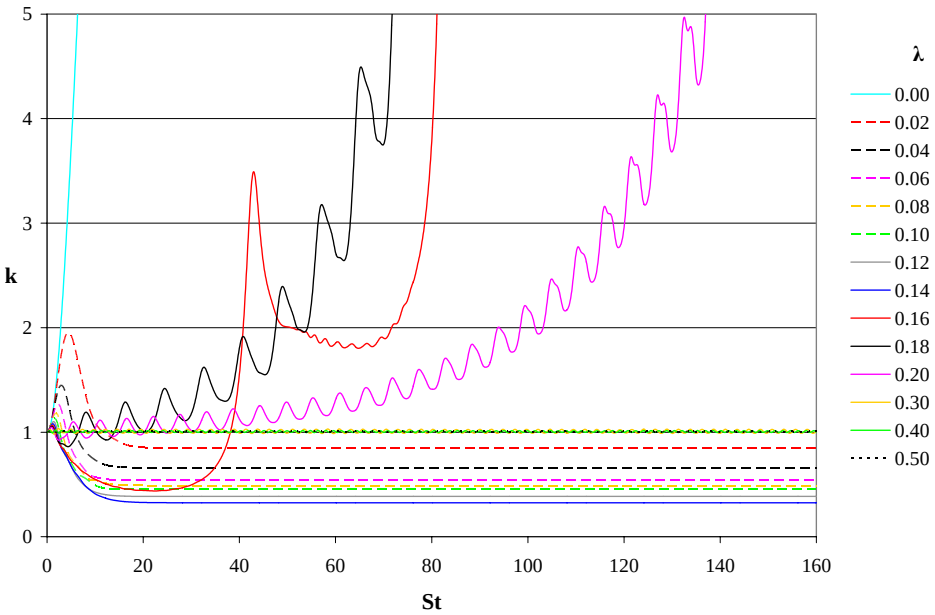

Fig. 13. Full RDT - Extended Kinetic Energy Evolution

portant result from the RDT calculations. It is clear from the evolution data that there is a significant difference in the predicted behavior of the turbulent velocity field between the Inertial Model and full RDT when considering periodically-forced turbulence. While the Inertial Model predicts bounded periodic evolution of the turbulent kinetic energy, full RDT results show a number of different types responses for the evolution of k. This also leads to the observation that not only are there differences in the responses between RDT and the Inertial Model, but also, for the RDT results themselves, there are significant differences in the responses of the turbulence to the different frequencies of forcing, not only quantitatively as in the Inertial Model, but also qualitatively.

Figures 14-16 below show the results for the evolution of the kinetic energy for a shorter time interval and for different scales of magnification to show more closely the different responses that are observed. An initial observation can be made in

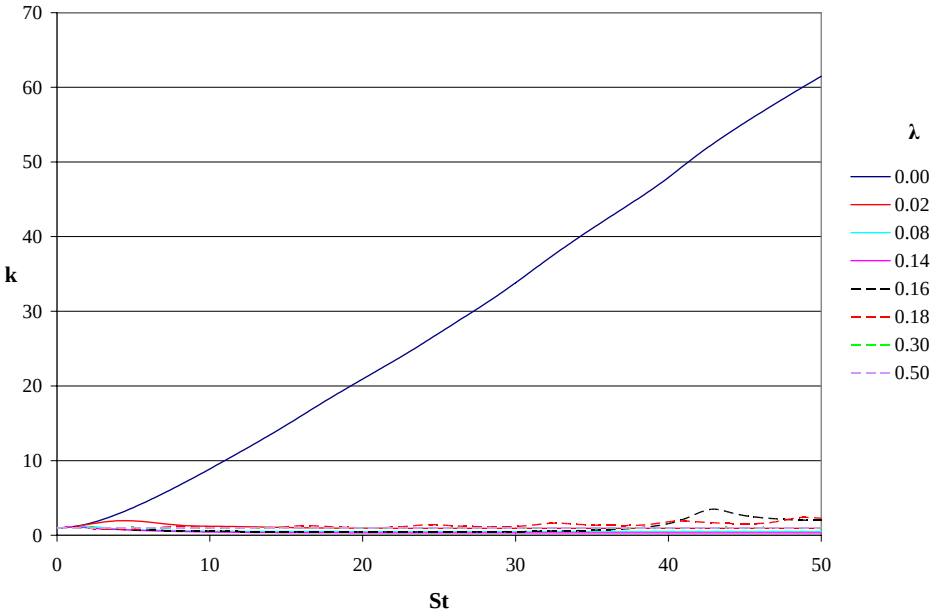

Fig. 14. Full RDT - Kinetic Energy Evolution (Large Scale)

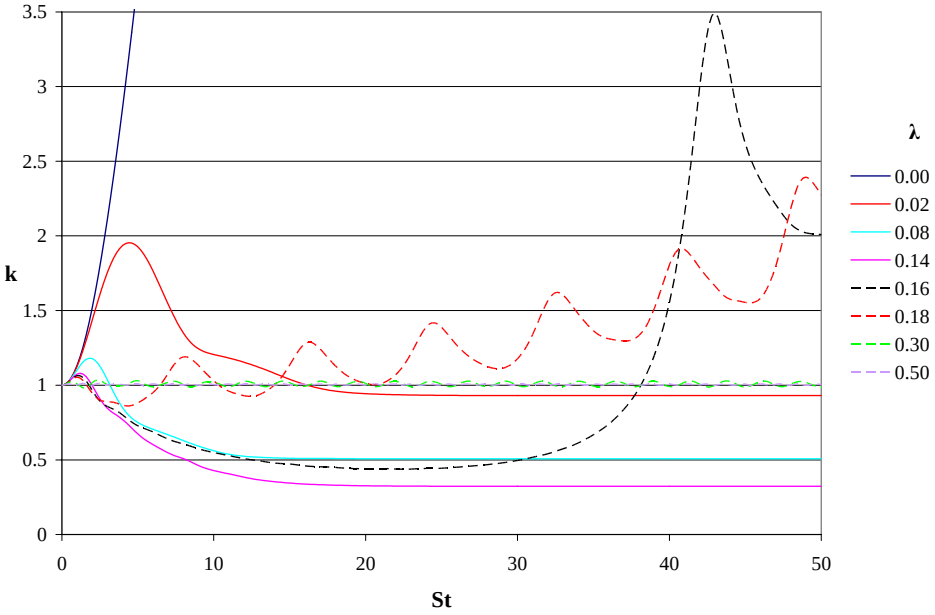

Fig. 15. Full RDT - Kinetic Energy Evolution (Medium Scale)

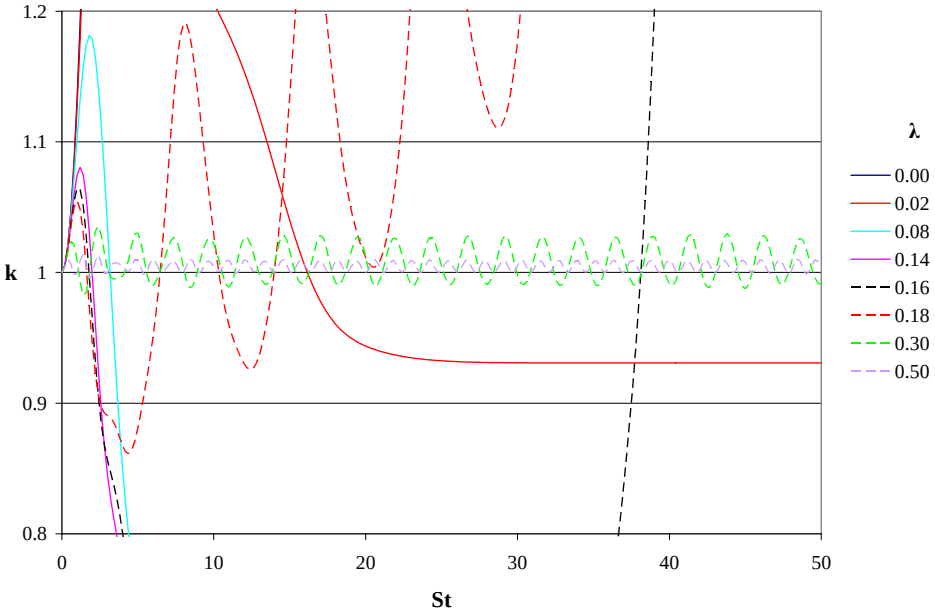

Fig. 16. Full RDT - Kinetic Energy Evolution (Small Scale)

Figure 14 concerning the homogeneous shear ($\lambda = 0$) distortion case in RDT. As discussed at the beginning of this chapter, the figure shows that, as with the Inertial Model case, the turbulent kinetic energy increases without bound for the zero forcing frequency (homogenous shear) case. Again, this growth appears to be asymptotically linear as opposed to the exponential growth predicted by the Inertial Model, and again, this is due to the influence of the rapid pressure, and it is the expected result in homogeneous shear RDT. (For more details see Pope (2000).)

In considering the periodic forcing cases ($\lambda > 0$), the evolution of the turbulent kinetic energy for full RDT is most effectively shown in figures 13, 15 and 16. For these nonzero forcing cases, the results indicate that there are several different categories of responses for different forcing frequencies. The differences in the evolution trajectories are extreme in some cases, and this is shown most effectively in Figure 13, where the data for all the frequencies that were calculated is presented for an extended time period. Again, the differences in response present a clear contrast to the Inertial Model, which predicts regular periodic behavior for all forcing frequencies. Figures 15 and 16 show 'close ups' of the nonzero forcing cases. The different types of response seem to characterize different ranges of forcing frequencies, and therefore can be looked at as different 'regimes' of response.

a. Low Frequency Regime

Looking at the data, especially in figures 13 and 15, it is clear that for the lower frequency cases, the evolution of the turbulent kinetic energy is marked by a slight initial increase followed by a decrease and eventual convergence to a constant value. This converged value for the kinetic energy evolution decreases as the forcing frequency λ increases. This evolution behavior characterizes the response of the turbulent velocity field for the reported forcing frequencies of $\lambda = 0.2, 0.8$, and 0.14, and all of

the intermediate frequencies in this range that were calculated, but not included in the figures. (See Table I) This set of frequencies that exhibit the same qualitative response for turbulent kinetic energy evolution can be considered as a 'low frequency regime' of behavior that is characterized especially by convergence to a constant value of k.

Recalling the RDT equation for the evolution of Reynolds stresses (Eq.(2.30)) and keeping in mind that the Inertial Model predicts regular oscillatory response in the absence of rapid pressure, this convergence to a constant k implies that the influence of the rapid pressure tends to damp out the oscillations in kinetic energy caused by the production mechanism. For this regime of low frequency forcing, the rapid pressure is able to completely damp out the oscillations in the kinetic energy evolution, eventually driving the kinetic energy gradient to zero and causing the evolution to reach a steady state. In this way it can be seen that in the low frequency regime of periodically-forced turbulence the presence of the rapid pressure acts to completely counteract the production, negating its influence on the turbulent velocity field at later times.

b. Intermediate Frequency Regime

Looking again at the data presented in figures 13 and 15, it can be seen that as we consider forcing frequencies above $\lambda = 0.14$, we see a sudden change in the response. When we consider the evolution data for a forcing frequency of $\lambda = 0.16$, we see that at early times, the turbulent kinetic energy evolution exhibits a response that is similar to the that of the lower frequency cases. This includes a very slight initial increase, followed by a decrease and apparent convergence to a constant value. As the evolution proceeds, however, there is an early indication that there has been a significant change in behavior. This indication is the fact that the kinetic energy

evolution for this higher forcing frequency case actually appears to settle down to a value that his higher than the asymptotic value for the previous lower frequency. This is contrary to the previous trend found in the low frequency regime where the kinetic energy evolutions for cases with progressively increasing forcing frequencies converge to progressively lower values. Then, at even later times in the evolution for $\lambda = 0.16$, there is a much more pronounced difference in the evolution, as the kinetic energy exhibits a sudden and very sharp increase. Again, in figure 13 the evolution of turbulent kinetic energy is shown for much later times, and it is clear that for forcing frequencies above $\lambda = 0.14$ there is, at later times, a sudden and drastic increase in kinetic energy, as the evolution data quickly diverges to extremely large values. This behavior holds true for an 'intermediate frequency regime' of forcing frequencies, above $\lambda = 0.14$ and below $\lambda = 0.30$.

Again, keeping in mind the pure oscillatory nature of the turbulent kinetic energy evolution that was predicted by the Inertial Model, it is clear that the activity of the rapid pressure is somehow responsible for the unusual divergent behavior exhibited in this range of forcing frequencies. Unlike the low frequency regime, the specifics of the influence of the rapid pressure in causing this unusual evolution behavior are not immediately apparent.

c. High Frequency Regime

We can now look at figures 15 and 16 to examine more closely the behavior of the kinetic energy evolution at frequencies above $\lambda = 0.20$. In figure 15 among the selected frequencies of forcing that are reported, we have the evolution data for frequencies of $\lambda = 0.30$ and 0.50. Although it is difficult to infer any quantitative information for these frequencies, it is clear that they predict an evolution that at least remains in the vicinity of the initial value of unity for later times. In Figure 16 we see a 'zoomed in'

view of the kinetic energy evolution for a number of different frequency, most notably for $\lambda = 0.30$.

From the figures it is clear that while the evolution data for the low frequency regime exhibited a behavior that settled down to a constant value and intermediate frequency evolution showed sudden and dramatic increases, the kinetic energy at higher frequencies above $\lambda = 0.20$ neither converge to a constant value nor exhibit a sudden increase. Instead, it is apparent that the higher frequency forcing causes the kinetic energy respond in a regular, oscillatory fashion, remaining in the vicinity of the initial value of 1. It is important to note while the response of the low and intermediate forcing cases differed drastically from the evolution predicted by the Inertial Model, this evolution behavior predicted by full RDT for high frequency forcing is qualitatively very similar to the response predicted by the Inertial Model as shown previously, especially in figures 2 and 3. For this reason, it is useful to compare the RDT results with those of the Inertial Model for the turbulent kinetic energy evolution in the high forcing frequency cases. Figure 17 below compares the responses predicted by the two models for the case of a high forcing frequency of $\lambda = 0.50$. From the figure it is apparent that the full RDT calculations, which include the effects of rapid pressure, shows distinct qualitative similarities to the Inertial Model results. While the oscillatory behavior is very similar, the amplitude of the oscillations is smaller for the full RDT case. In this way, it appears firstly that the for high forcing frequencies, the role of the rapid pressure is significantly less pronounced since it does not appear to significantly alter the qualitative response, as it apparently does for the low and intermediate frequency cases. Secondly, it appears that the small influence that the rapid pressure does have in the high frequency cases serves to mainly to dampen the magnitude of the oscillations that are present.

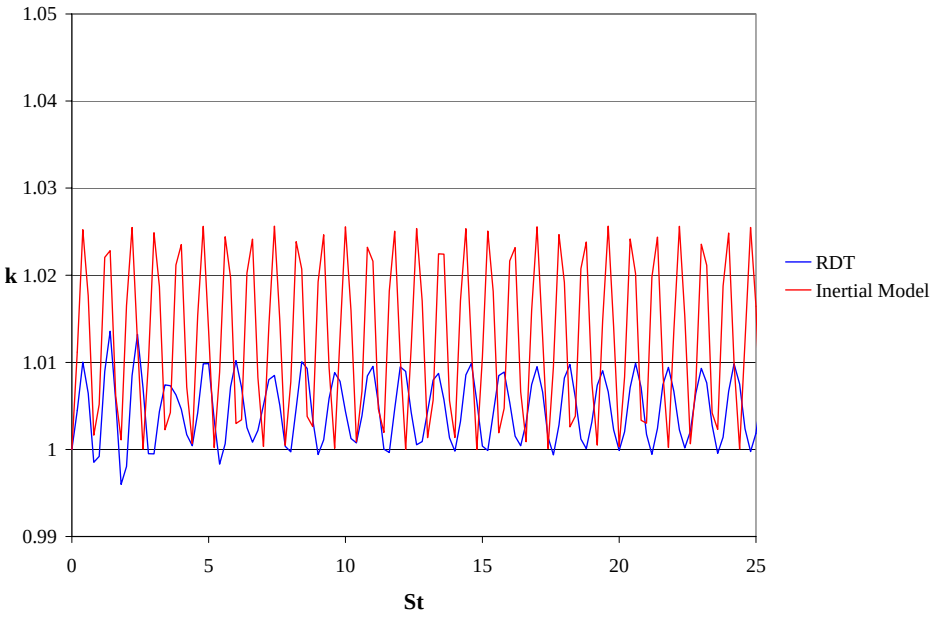

Fig. 17. Inertial Model vs. RDT - k Evolution for $\lambda = 0.50$

2. Reynolds Stress Anisotropy

The next parameter considered in the full RDT calculations for periodically-forced turbulence is the Reynolds-stress anisotropy. Figures 18-23 below show the evolution of the b_{11}, b_{22}, and b_{12} terms in the Reynolds stress anisotropy tensor. First, considering the constant homogeneous shear case ($\lambda = 0.0$), it is clear that the full RDT results for the evolution of the Reynolds stress anisotropies do not show a drastic difference in qualitative behavior when compared to the Inertial Model predictions (see Figs. 5-10). However, as with the turbulent kinetic energy evolution for the homogeneous shear case, there are certain quantitative differences. When compared to the Inertial Model, the full RDT results exhibit a behavior that can be best characterized as a 'damped' response for some components. Specifically, this is true for the b_{11} and b_{12} components, while the b_{22} component exhibits a nearly identical response to that predicted by Inertial Theory. Figure 24 below compares the responses for each of the

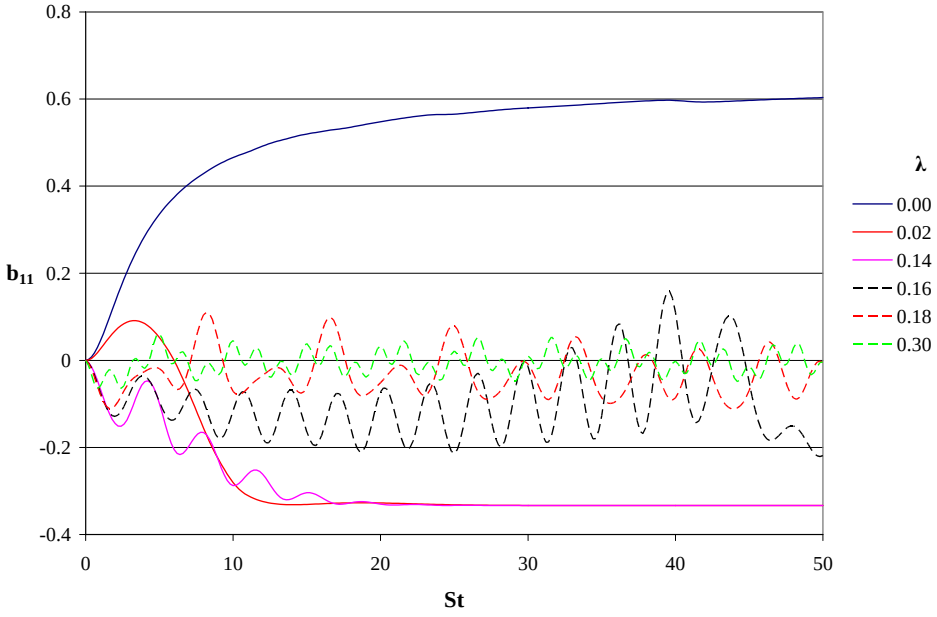

Fig. 18. Full RDT - b_{11} Evolution (Full View)

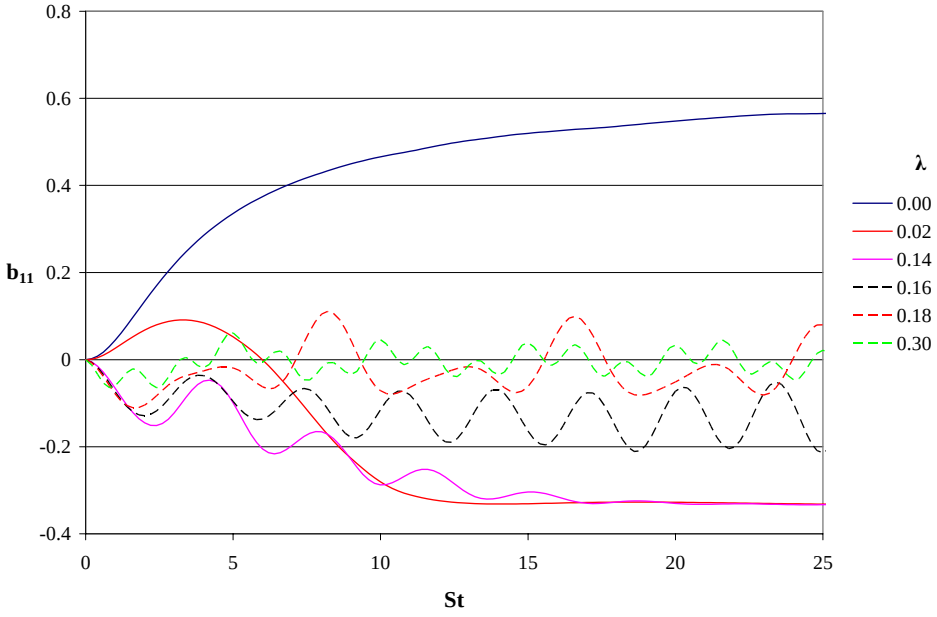

Fig. 19. Full RDT - b_{11} Evolution (Close-up View)

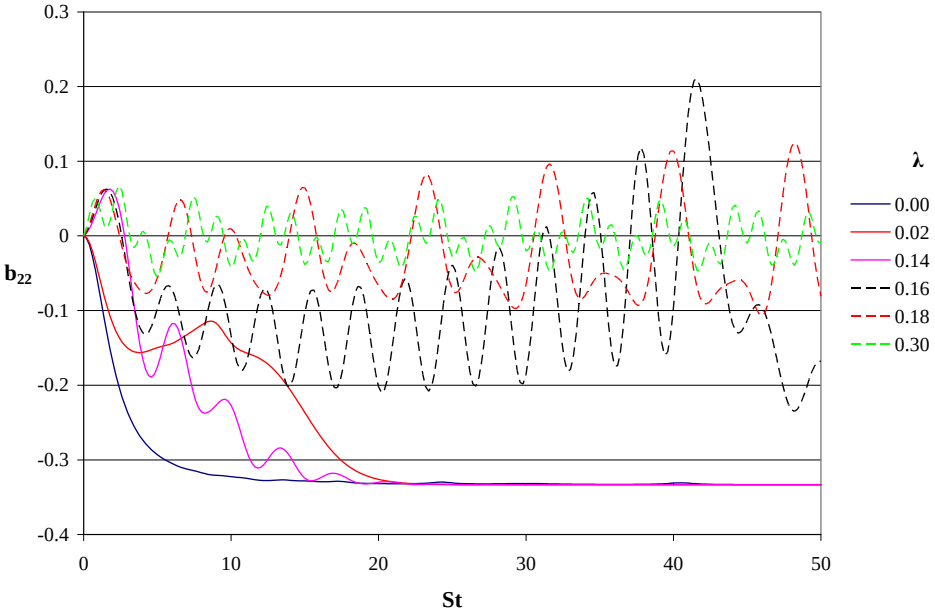

Fig. 20. Full RDT - b_{22} Evolution (Full View)

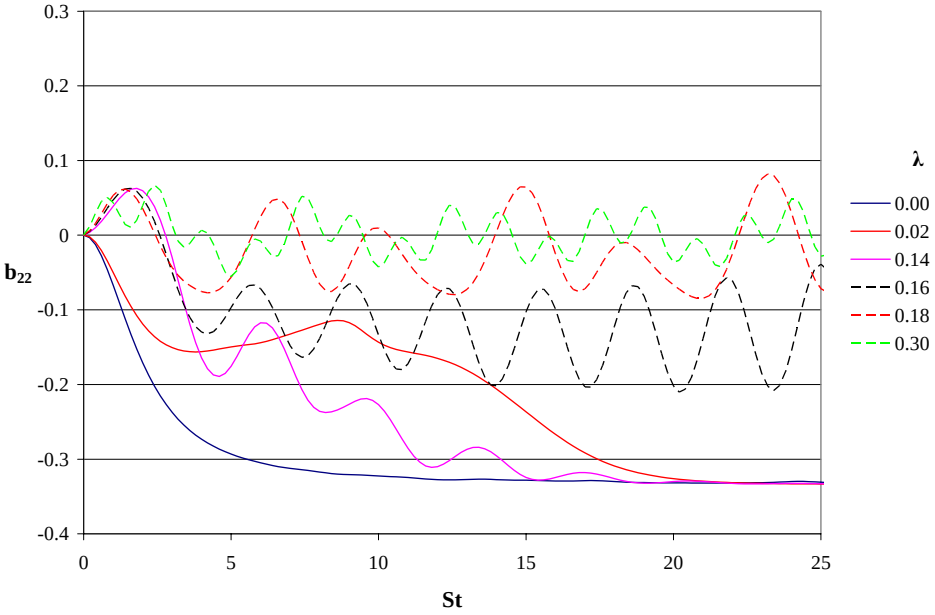

Fig. 21. Full RDT - b_{22} Evolution (Close-up View)

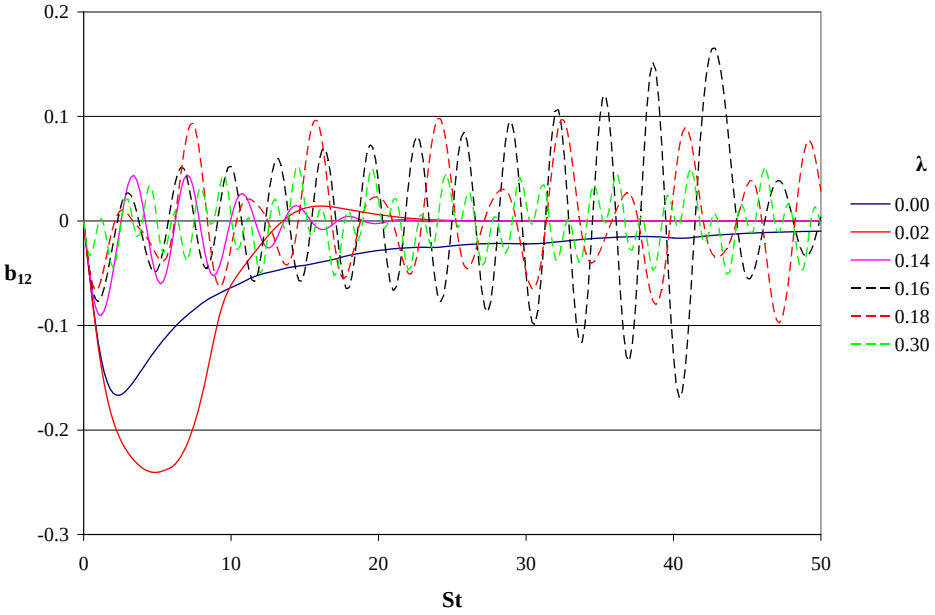

Fig. 22. Full RDT - b_{12} Evolution (Full View)

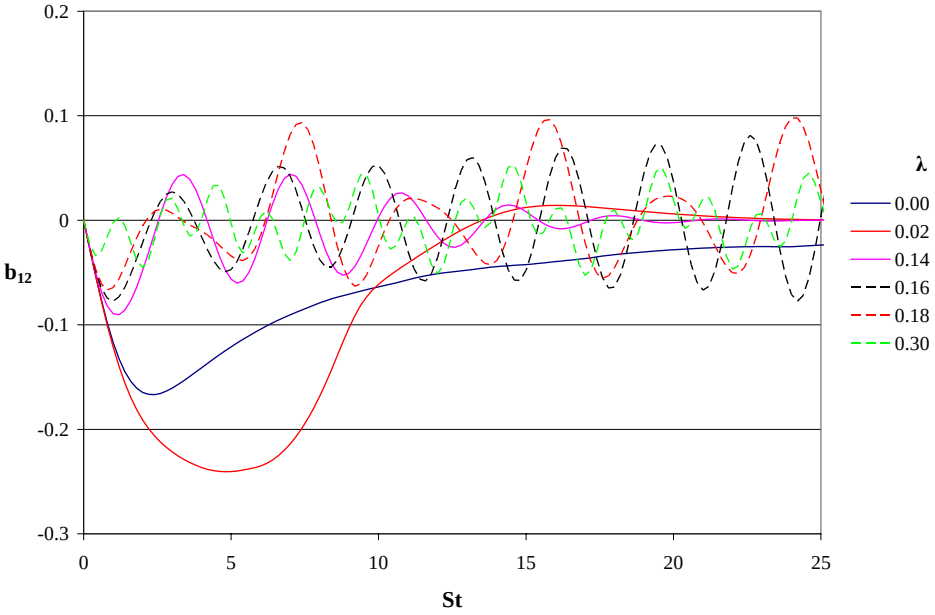

Fig. 23. Full RDT - b_{12} Evolution (Close-up View)

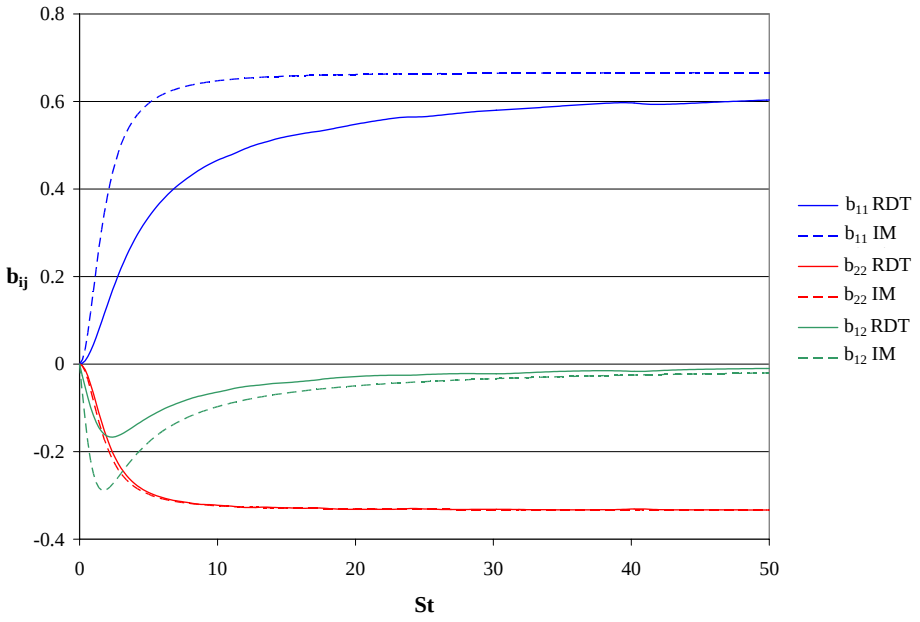

Fig. 24. Inertial Model vs. RDT - b_{ij} Evolution for Homo. Shear ($\lambda = 0$)

three components considered above for the zero forcing frequency case. This damped response predicted by full RDT is analogous to the results for the turbulent kinetic energy evolution, which also showed a damped response for the homogeneous shear in the full RDT calculation. It is another illustration of the role of rapid pressure in counteracting the influence of production.

Next, we consider the evolution of the Reynolds-stress anisotropies for the periodic-forcing cases ($\lambda > 0$). As with the kinetic energy evolution, the results in figures 18-23 indicate that there are several different behaviors present for the evolution of the anisotropies for different forcing frequencies. Thus, as with the kinetic energy evolution, the full RDT evolution data for the anisotropy components exhibit significant differences from the predictions of Inertial Theory. These differences can be divided into the same three regimes of low, intermediate, and high frequency response as defined for the turbulent kinetic energy.

Again, the results for the evolution of the anisotropy components display the same regime of coherent response for low frequency forcing as seen in the kinetic energy data. In the case of b_{11}, the evolution data for the low forcing frequency cases exhibit a convergence to a value of -1/3. Recalling the definition of b_{ij} (Eq.(3.10)), this value that corresponds to the $\langle u_1 u_1 \rangle$ Reynolds stress converging to zero. The evolution of the b_{22} component exhibits the same response for the low frequencies, converging to a value of -1/3, which again implies that $\langle u_1 u_1 \rangle$ converges to zero. For the b_{12} component of the Reynolds stress anisotropy tensor, the response for the low forcing frequency case exhibits a convergence to a value of zero. For this off-diagonal component, this also corresponds to the corresponding Reynolds Stress $\langle u_1 u_2 \rangle$ converging to zero. These RDT results for the evolution of b_{11}, b_{22}, and b_{12} are in contrast to the Inertial Model results shown in figures 5-10 that show an oscillatory response for the anisotropy components for all forcing frequencies. This again shows the influence of the rapid pressure at low forcing frequencies, and implies that its activity serves to damp out the oscillations in the Reynolds stresses.

As the forcing frequencies above $\lambda = 0.14$ are considered, we are in the 'intermediate frequency regime' where the results for the kinetic energy evolution have already shown that there is a drastic change in the response of the turbulent velocity field due to the periodic forcing. Recall once again that the Inertial Model predicts a well-behaved periodic response for the evolution of the Reynolds-stress anisotropy for all frequencies of forcing, including the intermediate regime. Now for the full RDT calculations in this regime we see oscillatory behavior that is clearly not as predicted for any of the components shown. For the b_{11} component, while the behavior is irregular, there are no apparent drastic increases in the evolution, as the amplitude of the oscillations remains comparable to that predicted by the Inertial Model calculations. For both the b_{22} and b_{12} components, however, we do see dramatic increases in the

amplitude of the oscillations, which correspond to the dramatic increases observed in the kinetic energy evolution (see figure 15). This response is most evident in the evolution of the b_{12} component, as the amplitude of the oscillations increases markedly over time. As with the results for the kinetic energy evolution, the drastic changes in response seen in the intermediate frequency range are understood as the result of the activity of the rapid pressure. Again, it is not immediately apparent how the action of the rapid pressure causes the velocity field to exhibit this behavior.

For forcing frequencies in the 'high frequency' regime (above $\lambda = 0.20$), there is again a different characteristic response that is present. Again, the evolution data for the anisotropy components exhibits a high frequency behavior that is analogous to the distinct high frequency results for the kinetic energy evolution. That is, while the evolution of the anisotropy components showed convergence to a constant value for low frequency forcing and marked increases and irregular behavior for the intermediate frequencies, the evolution of the high frequency forcing case predicts an evolution behavior that is qualitatively very similar to the response predicted by the Inertial Model (see figures 5-10). Specifically, at higher forcing frequencies the anisotropy components respond in a periodic fashion, oscillating about the initial value of zero, with an amplitude slightly less than that predicted by the Inertial Model. Figure 25 below compares the responses predicted by RDT and the Inertial Model for the b_{11} component of the Reynolds-stress anisotropy tensor at the high forcing frequency of 0.50.

As with the full RDT results for the evolution of the kinetic energy, we again see that the role of the rapid pressure in the high frequency regime is significantly less pronounced. Again, it does not appear to alter the qualitative response of the turbulent velocity field significantly, unlike low and intermediate frequency regimes. In addition, as with the kinetic energy evolution, the data indicates that the little

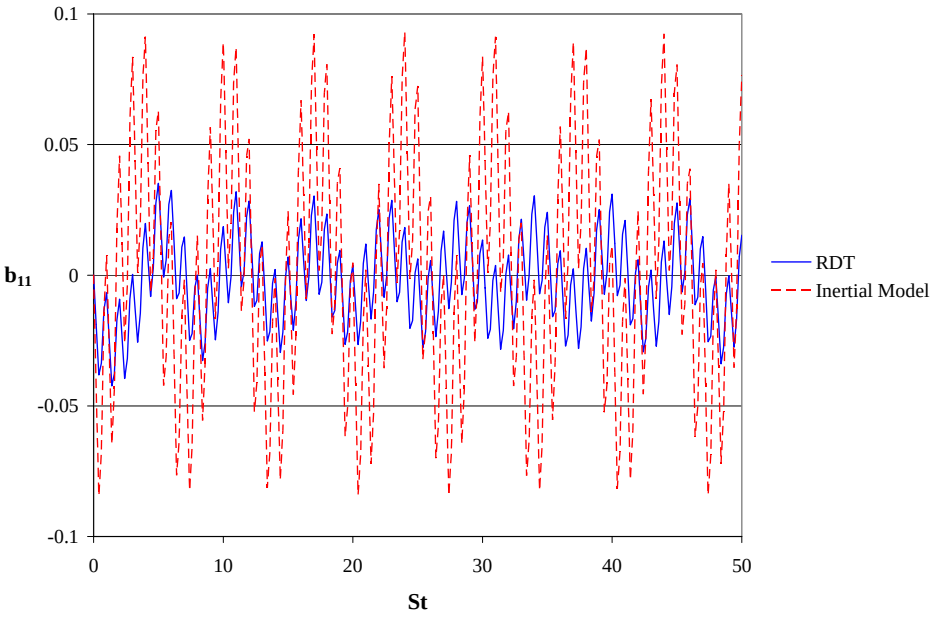

Fig. 25. Inertial Model vs. RDT - b_{11} Evolution for $\lambda = 0.50$

influence that the rapid pressure does have serves mainly to dampen the magnitude of the oscillations of the Reynolds-stress anisotropy components.

3. Turbulent Production

The next parameter considered in the full RDT calculations of periodically-forced turbulence is the turbulent production. Recall that the effect of the production in the absence of the effects of the rapid pressure was examined in the Inertial Model calculations, presented earlier in this chapter. In the full RDT calculation, the effects of rapid pressure are present, and thus we consider the behavior of production in the presence of the response of the turbulent velocity field. Figure 26 below shows the full RDT results for the evolution of the P_{11} component of production for the several different frequencies of forcing.

The same type of distinctions from the Inertial Model that were found in the

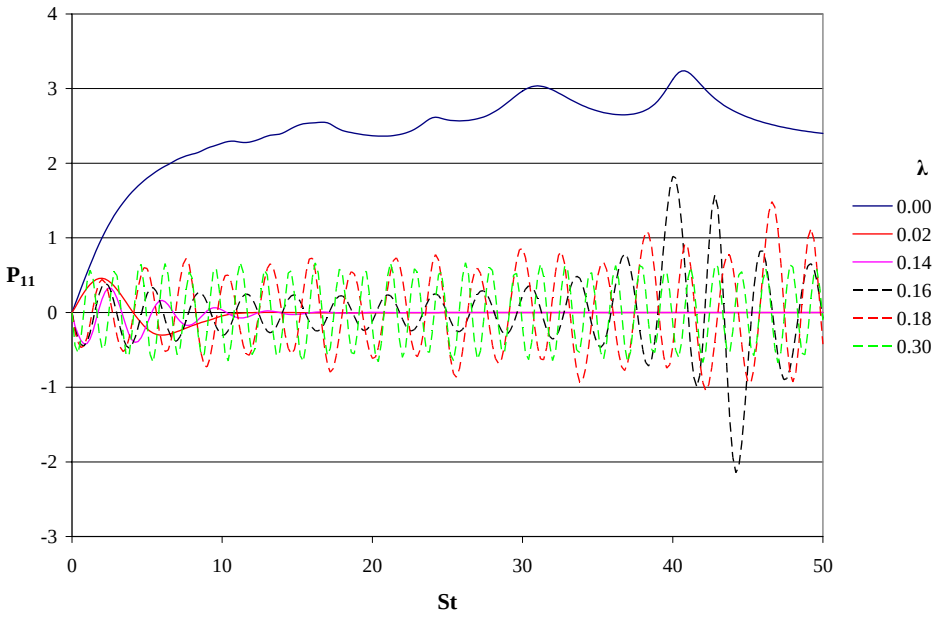

Fig. 26. Full RDT - Evolution of P_{11}

evolution of kinetic energy and anisotropy components are also noted in the full RDT production data. This includes the three distinct regimes of response to the unsteady forcing, as well as differences in the homogeneous shear response.

For the homogeneous shear ($\lambda = 0.0$) case, the Inertial Model predicts a perfectly linear increase for P_{11} since the only independent quantity in the model (see equations 2.32 and 2.36) is the applied mean flow gradient, and this is specified as a constant in homogeneous shear distortion case. The results for the full RDT model show the P_{11} component increasing initially, but leveling off at a constant value that is low in comparison to the values predicted by the linearly increasing Inertial Model. This is a response analogous to that seen for the kinetic energy evolution where the Inertial Model predicted parabolic increase while full RDT results exhibited a linear evolution with a much smaller magnitude. The evolution of P_{11} then then exhibits some unsteady behavior at later times. Overall, this behavior further illustrates

the impact of the rapid pressure on the evolution of the turbulent velocity field. The production term is dependent upon the Reynolds stresses, and since the rapid pressure alters the response of the Reynolds stresses, this in turn causes the production to have a different response for full RDT than for the Inertial Model.

For the periodic forcing cases we again see evolution behavior for P_{11} that corresponds the three regimes of response already discussed. Looking again at figure 26 we see that for the low frequency regime, the P_{11} evolution shows a convergence to zero. In the intermediate frequency regime the values no longer die out, but show significant increases in amplitude that correspond with the results for the other parameters considered above. For the high frequency cases, the response is again very similar to that predicted by the Inertial Model. In fact for the evolution of P_{11}, the full RDT results are not only qualitatively very similar to the Inertial Model results, but they are also very similar quantitatively. The high frequency evolution data for P_{11} for the Inertial Model and the full RDT calculation are compared in Figure 27.

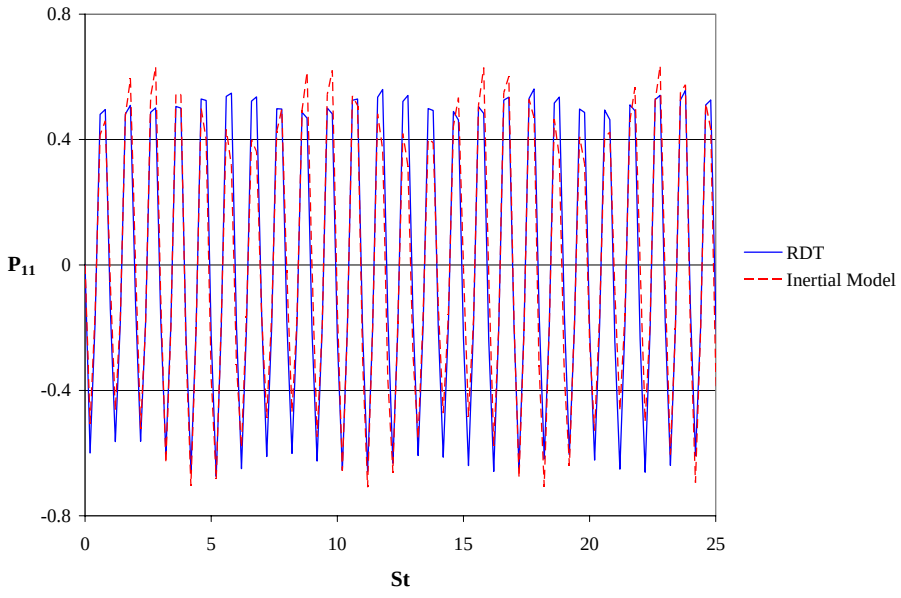

Fig. 27. Inertial Model vs. RDT - P_{11} Evolution for $\lambda = 0.50$

It is clear from the figure that at high frequencies, the evolution of the production is effected very little by the activity of the rapid pressure. Of all the parameters considered here, this data for the evolution of the production is the most illustrative of the reduced role of rapid pressure at high forcing frequencies.

4. Rapid Pressure-Strain Correlation

Finally we consider the full RDT results for the evolution of the rapid pressure-strain correlation term. As has been stated, the rapid pressure represents the straining reaction of the turbulent flow field when it is subjected to rapid distortion, in this case, periodic forcing. The results of the RDT calculation for the evolution of the R_{11} term of the rapid pressure for different forcing frequencies are shown in Figure 28.

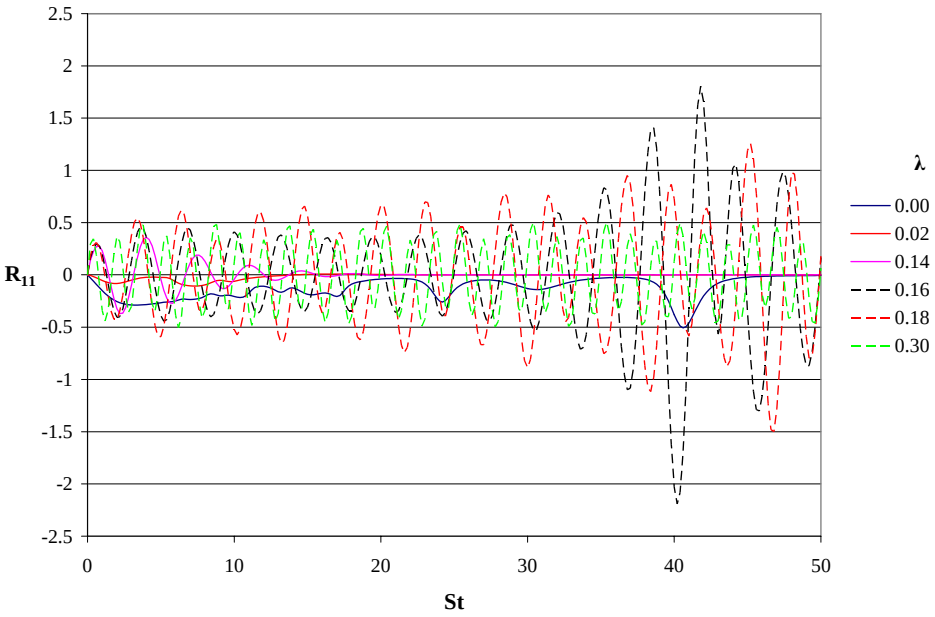

Fig. 28. Full RDT - Evolution of R_{11}

Because the Inertial Model omits the rapid pressure term, there are obviously no Inertial Model results with which to compare the results in Figure 28. However, the

results for the rapid pressure evolution are again similar to the previous RDT results.

For the homogeneous shear case, the rapid pressure remains in the vicinity of zero for all components, with a number of apparent instabilities that seem to correspond to instabilities seen in the production evolution. We have already seen that the production converges to a relatively steady behavior. Recalling that the gradient of the Reynolds stresses is dependent upon the sum of the production and the rapid pressure (Eq. (2.34)), this evolution behavior for R_{11} is consistent with the linear increase in kinetic energy for the RDT case that we have already seen.

Looking again at figure 28 and considering the nonzero forcing cases, we find the expected three regimes that we have already seen for the RDT calculation of the the other parameters in the velocity field. Specifically we find that the full RDT results for the evolution of R_{11} for periodically-forced turbulence exhibit three distinct regimes of behavior, with the evolution associated with increasing forcing frequencies characterized progressively by decay, growth, and periodic response.

CHAPTER V

DISCUSSION

In the previous chapter, the results from both the Inertial Model and full RDT calculations were presented. The data shows that for relatively low forcing frequencies, the effect of the rapid pressure on the velocity field is the greatest, as it is able to completely damp out the oscillations in the flowfield. As the forcing frequency is increased, the influence of the rapid pressure becomes weaker, and the damping of the oscillations in the velocity field becomes less and less effective. As the forcing frequency is increased further, a range of frequencies is reached where the damping action of the rapid pressure appears to become insufficient to completely damp out the oscillations in the velocity field and these oscillations appear to grow drastically. Finally, at even higher forcing frequencies, the influence of the rapid pressure appears to become insignificant, as the oscillations in the velocity field exhibit purely periodic behavior consistent with the forcing itself, and with the Inertial Model, which omits the role of the rapid pressure.

Thus, from the data that was shown, it is clear that full RDT predicts three different regimes of response for the periodic forcing case, and these regimes are directly dependent on the forcing frequency. More notable is the fact that while these different regimes of response were evident in the full RDT case, the Inertial Model predicted consistent response across all forcing frequencies. This difference implies that the distinct regimes of response that are predicted by RDT are dependent in some way on the effect of the rapid pressure, since it is the absence of this term that characterizes the Inertial Model. In a physical sense, that is to say that it is the relationship between the applied strain and the response in the velocity field that somehow causes it to respond differently under different forcing regimes. Specifically,

existence of three regimes of response implies that the influence of the rapid pressure in the presence of unsteady forcing causes the velocity field to exhibit three different types of relationships between the applied distortion and the resulting strain in the velocity field.

To better illustrate this behavior it is useful to consider the evolution of the turbulent kinetic energy. As shown in figure 15 in the previous chapter, the kinetic energy evolution very clearly exhibits the existence of the three regimes of response. Now consider the equation for the evolution of the turbulent kinetic energy in RDT. To derive this equation it is necessary first to consider the evolution equation for the Reynolds stresses, first given in Chapter II (Eq. (2.30)):

$$\frac{\partial}{\partial t}\langle u_i u_j\rangle = -\langle u_j u_k\rangle \frac{\partial\langle U_i\rangle}{\partial x_k} - \langle u_i u_k\rangle \frac{\partial\langle U_j\rangle}{\partial x_k} + 2\frac{\partial\langle U_l\rangle}{\partial x_k}(M_{kjil} + M_{ikjl}) \tag{5.1}$$

Now keeping in mind the definition of M_{ijkl} (Eq.(2.31)), also given in Chapter II, and recalling the definition of the turbulent kinetic energy, given in equation (3.9) the equation for the evolution of the kinetic energy can be obtained from the above equation:

$$\frac{\partial k}{\partial t} = -2kb_{ij}S_{ij}. \tag{5.2}$$

This equation further illustrates the relationship between the applied distortion (contained in the S_{ij} tensor), and the response of the flow (contained in the anisotropy tensor, b_{ij}). Figures 29 and 30 below show the full RDT results for the evolution of the (1,1) component of the b_{ij} and S_{ij} tensors for two different forcing frequencies. Looking at the results in the figures, we see that the evolutions for b_{ij} and S_{ij} are oscillatory (with nearly the same time period), and that there is an apparent phase lag between them. This data suggests that the evolutions of b_{ij} and S_{ij} can be modeled

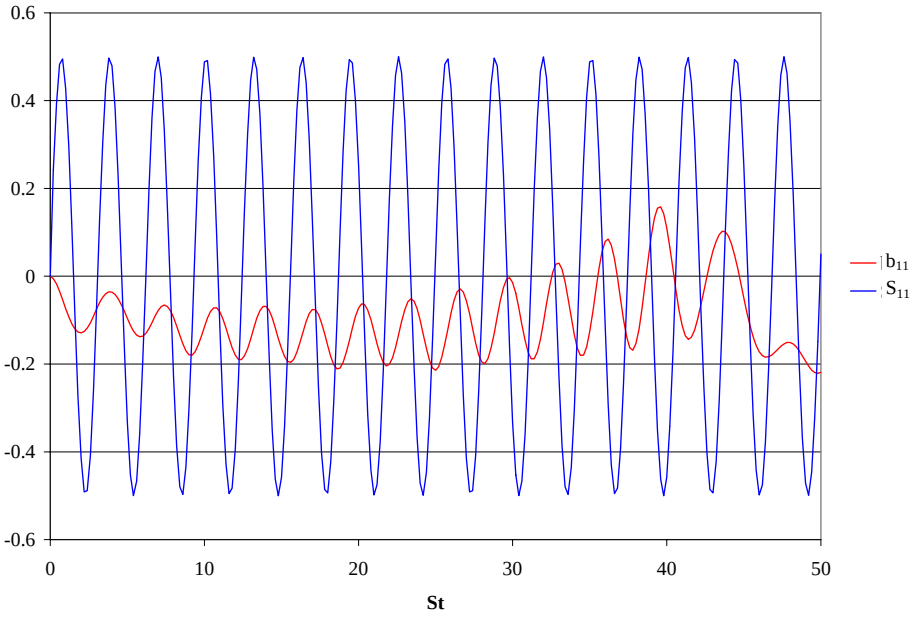

Fig. 29. Full RDT - Evolution of b_{11} and S_{11} for $\lambda = 0.16$

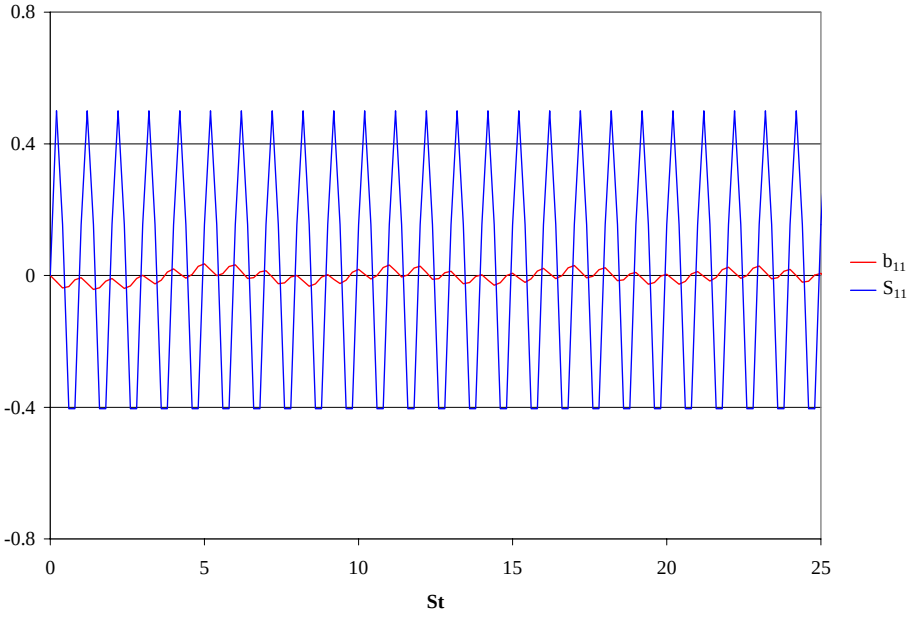

Fig. 30. Full RDT - Evolution of b_{11} and S_{11} for $\lambda = 0.50$

as trigonometric functions, separated by some finite phase lag. In this manner, the following simple model for the turbulent kinetic energy evolution is proposed:

$$\frac{\partial k}{\partial t} = -kcos(\theta)cos(\theta + \alpha) \tag{5.3}$$

This equation is analogous to equation (5.2), with the S_{ij} term modeled as $cos(\theta)$ and the b_{ij} term modeled as $cos(\theta + \alpha)$. In this equation, α is some constant phase lag. When the above model is integrated, we obtain the following evolution equation for the kinetic energy:

$$k(t) = e^{-\frac{1}{2}cos(\alpha)t - \frac{1}{4}sin(2t+\alpha) + \frac{1}{4}sin(\alpha)} \tag{5.4}$$

Thus, if we consider a specific case with a given value for the phase lag between stress and strain, the above equation gives the evolution of the kinetic energy for our model. Figure 31 gives the evolution of k according to equation (5.4) for several values of α. The results in the figure are remarkable because they show that for the simple model

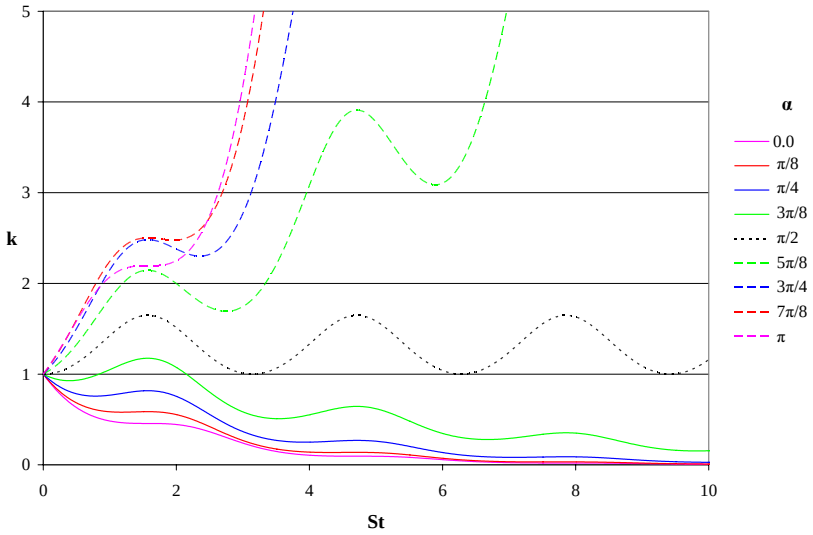

Fig. 31. Evolution of k for various values of phase lag, α

that was proposed above, we see three regimes of behavior for the kinetic energy. This closely resembles the results given in the previous chapter for the kinetic energy evolution, which also exhibited three distinct regimes of behavior.

In order to relate the behavior of this simple model to the actual results for unsteadily-forced turbulence predicted by RDT, we look again at the RDT data. We have already seen that for high forcing frequencies, the influence of the rapid pressure disappears and we are left with a periodic response in the velocity field. Looking at figure 30 we see this periodic response in terms of b_{11}, and in this data set it is clear that there is a phase lag of $\pi/2$ between b_{11} and S_{11}. That is, when the effects of rapid pressure are negligible, there seems to be a phase lag of $\pi/2$ between the applied distortion and the straining response of the velocity field. In addition, the data obtained in the previous chapter for both the Inertial Model (Fig. 4) and RDT at high frequency (Fig. 16) shows that the kinetic energy is oscillatory with a minimum value of unity. This behavior is captured well in the proposed model. We see in Fig. 31 that if there is a phase lag of $\pi/2$ between b_{ij} and S_{ij} the model predicts a purely oscillatory response for the kinetic energy, with the initial value of unity as a minimum.

Referring again to the RDT results, we consider the case where the effects of rapid pressure are the strongest. As we have already seen, this corresponds to the low forcing frequency cases where rapid pressure is able to completely damp out all oscillations in the flow. The RDT data shows that the effects of rapid pressure are strongest at the slowest of forcing frequencies, as oscillations are damped out most quickly in these cases. As the forcing frequency is increased, the oscillations are damped out less and less effectively. Again, this behavior seems to be captured very effectively by the model proposed above. In phase lag values ranging from 0 to $\pi/2$ we see a highly damped response, with oscillations in the kinetic energy damping

out to zero. We also observe in this model the phenomena of decreased damping effectiveness with increased values of phase lag. Recall that we have already seen that in the absence of the effects of rapid pressure we see a phase lag of $\pi/2$ between b_{ij} and S_{ij}. Therefore any action of the rapid pressure would be to alter this phase lag, so that a value of α close to $\pi/2$ would correspond to the rapid pressure having small influence. Looking again at Fig. 31 we see that for values of α ranging from 0 to $\pi/2$, those values closest to zero show a highly damped behavior while those very close to $\pi/2$ exhibit the least effective damping of the kinetic energy.

Finally we consider the RDT results for forcing frequencies where the effects of rapid pressure are present, but they are not sufficient to completely damp out the responses in the velocity field. These frequencies correspond to the 'intermediate regime' specified in the previous chapter. In the RDT data for these frequencies, we see an initial oscillatory response that shows little or no damping, followed by a sudden increase in the amplitude of the oscillations. In the model proposed above, we see that for phase lag in the range from $\pi/2$ to π, the model predicts oscillations that increase drastically in magnitude. However, we have already demonstrated that for the proposed model, the influence of rapid pressure range from zero effect, which corresponds to a phase lag value of $\pi/2$ to greatest effect which corresponds to phase lag values approaching zero. It is not immediately clear how the rapid pressure can directly cause the velocity field to experience a phase lag of greater than $\pi/2$ when the limiting case for zero effect of rapid pressure corresponds to a phase lag of $\pi/2$.

Overall, the different regimes of phase lag for the simple proposed model above are illustrated in figure 32 below. The figure shows the range of phase lag values outlined above and illustrates the corresponding regimes of behavior and the relative influence of rapid pressure. In order to explain the physical results seen in RDT in terms of the model proposed above, it is postulated that for a given value of the forcing

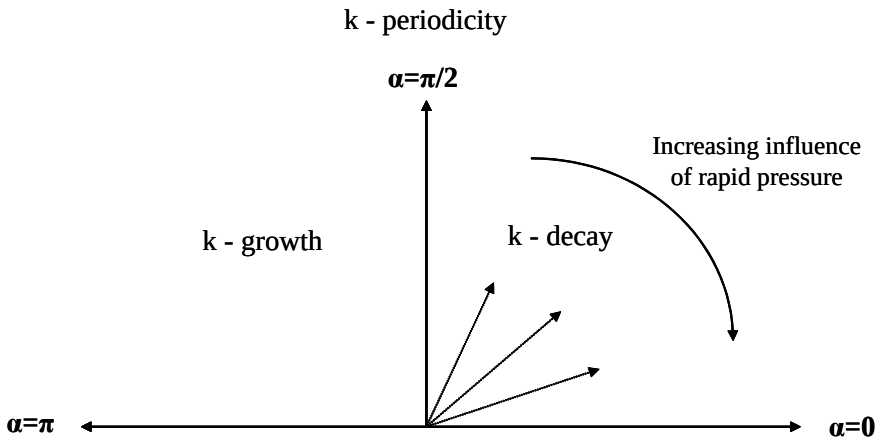

Fig. 32. Regimes of behavior for α

frequency, the rapid pressure allows for a range of values for the actual lag between b_{ij} and S_{ij}. The size of the range may depend upon the forcing frequency. At very high and very low frequencies this range is small, but at intermediate frequencies, it may be larger. It is also observed that this lag can vary over time as the flow evolves. For the very low frequency cases, the corresponding values allowed for α are all close to zero, and they are all readily damped out by the rapid pressure itself. As we consider higher forcing frequencies we move to values of α that are closer and closer to the limit of $\pi/2$. At some frequency sufficiently close to this limit, the range of values for α that are 'permitted' by the rapid pressure include those that are greater than $\pi/2$, and when the oscillations cross into this region we observe the dramatic increases in amplitude that characterize the intermediate regime of response. In this manner the proposed model also captures the behavior of the velocity field as seen in 'intermediate regime' RDT results. Finally, when the forcing frequency is sufficiently high such that the effects of rapid pressure are negligible, the velocity field is 'forced' to remain on the $\pi/2$ limit, since the influence of the rapid pressure disappears.

The analysis outlined above implies that the role of rapid pressure in unsteadily forced turbulence serves to create a temporal lag between the applied distortion and the strain in the flow. For different frequencies of forcing, this phase lag can take on different values, and depending on the amount of lag that is present between stress and strain, we see different responses in the turbulent velocity field. The results of the present study have already illustrated the existence of three regimes of response in the presence of periodic forcing. The simple model analysis above suggests that these regimes correspond to three distinct ranges of values for a phase lag between stress and strain that are caused by rapid pressure.

CHAPTER VI

SUMMARY AND CONCLUSIONS

In this study, the response of a turbulent velocity field to unsteady periodic forcing has been examined. The study was performed using Rapid Distortion Theory, a linear theory that provides for relatively affordable computation over a wide range of parameters. Calculations were performed for both full RDT and also the Inertial Model (which neglects the presence of the rapid pressure-strain correlation) to examine the role of rapid pressure in the observed RDT response. The the responses predicted by the Inertial Model were calculated first. For this case, the flow exhibited a consistent, steady, periodic response for all forcing frequencies. Next, the full RDT calculations were performed using various forcing frequencies, and the results showed that the velocity field exhibits three distinct types of responses to the periodic forcing. For relatively low frequencies, the velocity field settles down to a constant steady behavior, with all fluctuations dying out. In an intermediate frequency range, the velocity field exhibits sudden and drastic increases in kinetic energy. When subjected to higher forcing frequencies, the velocity field behaves in a simple periodic fashion, with all parameters oscillating around their initial condition. The differences in the predicted response between full RDT and the Inertial Model make it clear that the distinct regimes of behavior that are exhibited by the turbulent velocity field, as shown in the RDT calculations, are due to the effect of the rapid pressure. For low-frequency forcing, the effects of rapid pressure are the strongest and are sufficient to counteract production and completely damp out oscillations. In the intermediate regime of frequencies, the effects or rapid pressure are less pronounced, but are significant enough to cause the velocity field to exhibit sudden dramatic increases in the turbulent kinetic energy and other flow parameters. At relatively high frequen-

cies, the velocity field behaves in a manner very similar to that seen in the Inertial Model, with a constant, steady, periodic response. This implies that at these high frequencies, the qualitative effects of rapid pressure are significantly diminished.

In order to explain the observed behavior more specifically in terms of the interaction between applied stress and the straining response in the flow, the equation for the evolution of the kinetic energy was considered. Using this equation, a model was proposed that represents the stress and strain as trigonometric functions with a phase lag. Calculations using this model produce results that closely resemble the results of the RDT calculations. For this model we see the existence of three distinct regimes of behavior, according to different ranges of the phase lag. A value of $\pi/2$ for the phase lag leads to bounded periodic behavior of kinetic energy corresponding to the Inertial Model and RDT at high forcing frequencies. For phase lag values from zero to $\pi/2$ we see a damped response for the model, while those ranging from $\pi/2$ to π show a kinetic energy evolution that increases dramatically. It is proposed that phase lag values close to zero in the model correspond to the low forcing frequency regime in which the role of the rapid pressure is strongest and it is able to damp all oscillations in the flow. For values of the phase lag that approach the limiting value of $\pi/2$ (zero effect of rapid pressure) we see that the rapid pressure allows for oscillations can occasionally take values greater than $\pi/2$, causing sudden increases in oscillation that correspond to the dramatic increases seen in the intermediate regime of forcing seen in RDT. Overall, the results of the simple model verify that that differences in response first seen in the RDT calculations can be explained in great part as the effects of a 'lag' between stress and strain that is caused by the activity of the rapid pressure. Finally, it should be noted that while the calculations in the present study were performed for initially isotropic turbulence, we expect the behavior to be consistent for other initial conditions as well.

In summary, the main conclusions that can be drawn from the results of this study are:

(i.)Turbulence, when subjected to unsteady periodic forcing, exhibits three different regimes of response.

(ii.)The existence of the regimes is caused by the effect of rapid pressure.

(iii.)Rapid pressure serves to create a 'phase lag' between the applied stress and the straining in the velocity field, and this phase lag accounts in great part for the different regimes of response that are evident in periodically-forced turbulence.

REFERENCES

Bernard, P.S. & Wallace, J.M 2002 *Turbulent Flow.* John Wiley & Sons.

Crow, S. 1968 Viscoelastic properties of fine-grained turbulence. *J. Fluid Mech.* **33**, 1–20.

Girimaji, S.S., Jeong, E. & Poroseva, S.V. 2003 Pressure-strain correlation in homogeneous anisotropic turbulence subject to rapid strain-dominated distortion. *Physics of Fluids* **15**, 3209-3222.

Hunt, J.C.R. & Caruthers, D.J. 1949 Rapid distortion theory and the 'problems' of turbulence. *J. Fluid Mech.* **212**, 497–532.

Launder, B.E., Reece, G.J. & Rodi, W. 1973 Progress in the development of a Reynolds stress turbulent model. *J. Fluid Mech.* **68**, 537–566.

Maxey, M.R. 1982 Distortion of turbulence in flows with parallel streamlines. *J. Fluid Mech.* **124**, 261–282.

Pope, S.B. 2000 Rapid distortion theory. In *Turbulent Flows*, pp. 404–422. Cambridge University Press.

Sreenivasan, K.R. & Narasimha, R. 1977 Rapid distortion of axisymmetric turbulence. *J. Fluid Mech.* **84**, 497-516.

Taylor, G.I. & Batchelor, G.K. 1949 The effect of wire gauze on small disturbances in a uniform stream. *Quart. J. Appl. Math.* **2**, 1–26.

VITA

Joshua R. O'Neil was born in Houston, Texas in 1978. He was home schooled from the fifth grade through high school. He entered the University of St. Thomas in Houston in 1996 and attended for three years studying mathematics. Subsequently, in 1999 he entered Texas A&M University to study Aerospace Engineering. In 2002 he concurrently received his Bachelor of Arts in Mathematics from the University of St. Thomas and his Bachelor of Science in Aerospace Engineering from Texas A&M University. Mr. O'Neil can be reached at the following address: 5740 Fontenelle, Houston TX, 77035.